NASA CR-143746

15 JANUARY 1975

EXPERIMENT DEFINITION PHASE SHUTTLE LABORATORY

LDRL-10.6 EXPERIMENT

•

Second Quarterly Report

NASA Contract NAS 5-20018

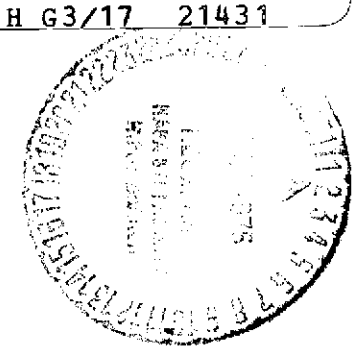

HUGHES
HUGHES AIRCRAFT COMPANY
SPACE AND COMMUNICATIONS GROUP

Hughes Ref. No. D0824 • SCG 50039R

CONTENTS

ILLUSTRATIONS

TABLES

1. INTRODUCTION AND SUMMARY

The second quarterly report for the Experiment Definition Phase of the Shuttle Laboratory LDRL-10.6 Experiment (Contract No. NAS 5-20018) covers the activities from 26 September to 26 December 1974. A crucial event for the program occurred in the meeting with the customer on 25 September 1974 at Goddard Space Flight Center. It was realized that the first experimental deployment of LDRL-10.6 link in space will be between a shuttle transmitting terminal and an elliptical orbit satellite or a ground receiving terminal. This, in turn, implied a change in the scope of the program. It was decided that by restricting to two the number of links to be investigated, and adding an additional $200,000.00 to the present contract, it would be possible to do the following:

- Design the LDRL-10.6 experiment for the shuttle to ground and shuttle to elliptical orbit
- Fabricate and deliver the 10 μm optomechanical (OM) subsystem brassboard model

With this guideline, a new program plan was prepared and submitted for customer approval in the monthly report covering the period 26 September to 26 October 1974. Initial work for the experimental measurements on the optomechanical subsystem for the 10 μm receiver also have been started during October. The authorization for proceeding on the new program plan was received 9 January 1975 from the GSFC technical officer.

The subject of the OM subsystem definition for the shuttle transmitting terminal was the main effort during November. Optical analysis for the Gregorian telescope was also started, and alternatives to gimbal drives and IMCs were examined.

In the month of December, the design of the OM subsystem was crystalized by completing the optical analysis and the weight optimization. The current view of the OM subsystem for the shuttle transmitter terminal is an 18 cm (nominally 7 inches) afocal Gregorian telescope in a two gimbal beryllium structure. The telescope rotates about its optical axis through an angle of ±97° (outer gimbal). A 45° large folding mirror placed after the primary focusing mirror directs the beam to the pointing mirror. The pointing mirror is also a 45° folding mirror that rotates about the beam axis through an

angle of ±75° (inner gimbal). In addition, provisions for beam steering control for establishing and maintaining the link with an elliptical orbit (Molniya) spacecraft 10 μm receiver (of 26 cm aperture), as well as with a ground station, are provided. Lead angle compensation and a nutating device for conical scan are also included in the receiver path, and beam expander and a broad beam illumination device are included in the transmitter path. The parameters of the OM subsystem for the shuttle terminal are summarized in Table 1-1.

Note that the shuttle OM subsystem design parameters are not the ones obtained for the spaceborne weight optimized system. Instead, at substantial cost savings, a suboptimal point was selected, which increased the optimal spaceborne weight by less than 2 pounds.

Observe that the weight optimization program was modified, as indicated in Section 2, so as to include, among other things, the obscuration as a function of aperture diameter for fixed field of view (FOV) and f number. This, in connection with the more detailed evaluation of system losses, resulted in the optimized values, indicated in Table 1-2, which differ from the ones reported in the first quarterly report.

Direct drive brush torque motors have been selected as the gimbal drives for the baseline design. An examination of the image motion compensation (IMC) requirements, particularly during acquisition, revealed the inadequacy of the currently available piezzoelectric GTE devices. It seems that an electromagnetic type of device is advisable. Further investigation of this topic, however, is beyond the objectives of the current project and will not be pursued.

The link establishment analysis indicated that the shuttle, as a direct carrying platform for the LDRL-10.6 shuttle transmitter, is unsuitable due to its excessive pointing accuracy of ±0.5°. The instrument pointing system (IPS), to be carried onboard the shuttle, may be utilized profitably as the carrying platform for the shuttle transmitter. Contact with G. C. Marshall Space Flight Center, Huntsville, Alabama has been established and the subject will be pursued next quarter.

TABLE 1-1. OM SUBSYSTEM PARAMETERS

Parameter	Value	Remarks
Aperture	18 cm	Primary mirror
Magnification	7x	
Diameter obscuration ratio	0.412	Primary mirror
F number	1.5	
Acquisition field of view*	±0.5 deg	
Coverage	Near hemispherical	±15° cone about the outer gimbal axis is not covered
Tracking rate (maximum)	0.8 deg sec^{-1}	
Gimbal pointing accuracy	±0.02 deg	
IMC mirror size	2.54 x 3.6 cm	Elliptical

*This is a design goal for the operational deployment of the shuttle transmitter.

TABLE 1-2. DESIGN PARAMETERS FOR SPACEBORNE TERMINALS

Parameter	Shuttle Transmitter		Molniya Receiver	
	Chosen	Optimal	Chosen	Optimal
Aperture diameter, cm	18.0	20.1	26.1	25.5
Laser output power, W	1.05	0.956	–	–
Prime power required, W	198.8	192.8	159.2	159.1
Package weight, lb	111.7	115.6	129.1	126.4
Total spacecraft weight impact, lb	230.2	230.9	225.9	223.2

2. LINK ANALYSIS AND OPTIMIZATION

Systems analysis efforts during the second quarter have been directed toward the following activities:

1) A more refined assessment has been made of all factors that determine the link signal-to-noise ratio (S/N) budget. The results have been incorporated in the weight optimization computer program calculations and in a more detailed computer generated link Design Control Table. The weight optimization computer program (hereafter referred to as the Link Analysis Program) now has options for generating a link Design Control Table for any specified combinations of S/N, transmitter and receiver aperture diameters, and transmitter power.

2) The revised Link Analysis Program now performs S/N calculations using nominal, favorable, and adverse values for all link parameters and displays the corresponding favorable and adverse tolerances about each nominal entry in the computer generated Design Control Table.

3) The transmitter aperture obscuration required for specified field of view and system f number is now determined by the optimization program as a function of the transmitter aperture diameter.

4) The LDRL weight optimization has been revised in view of the foregoing revisions and enhancements to the system performance model.

5) Finally, the sensitivity of LDRL system weight and transmitter package weight to variations in transmitter aperture diameter about the optimum point has been examined. These results provide a firm basis for the necessarily subjective tradeoff between LDRL system weight and transmitter package cost.

2.1 LDRL-10.6 SIGNAL/NOISE CALCULATIONS

The refined LDRL-10.6 calculations are presented in the form of a Design Control Table, (Figure 2-1). The intermediate frequency signal-to-noise ratio $(S/N)_{IF}$ for an optical heterodyne receiver is given by

$$(S/N)_{IF} = \frac{\left(\frac{G\eta q}{h\nu_c}\right)^2 R_L P_S P_{LO}}{qB_{IF}G^2\left[\frac{\eta q}{h\nu_c}\left(P_S + P_B + P_{LO}\right) + I_D\right]R_L + 2k\,TB_{IF}} \qquad (2\text{-}1)$$

where

B_{IF} = intermediate frequency bandwidth

G = detector gain

η = detector quantum efficiency

q = electronic charge

h = Planck's constant

ν_c = optical carrier frequency

R_L = detector load resistance

P_S = received signal power

P_B = received background power

I_D = detector dark current

k = Boltzmann's constant

T = postamplifier noise temperature

P_{LO} = local oscillator power

For the ideal case in which the local oscillator power dominates the other noise terms in the denominator, this expression reduces to

$$(S/N)_{IF_{ideal}} = \frac{P_s\eta}{h\nu_c B_{IF}} \qquad (2\text{-}2)$$

TRANSMITTER PARAMETERS	NOMINAL	FAV. TOL.	ADV. TOL.
MODULATED LASER OUTPUT POWER(1.05W)	.23	.000	.000
BEAM EXPANDER LOSS.....	-.06	.006	-.006
DIPLEXER LOSS.....	-.41	.043	-.043
IMAGE MOTION COMPENSATOR LOSS.....	-.22	.022	-.022
OPTICS REFLECTANCE LOSSES.....	-.66	.134	-.133
OBSCURATION LOSS (GAMMA=.412).....	-3.43	.000	.000
POINTING LOSS.....	.00	.000	-.079
IDEAL APERTURE GAIN(.180M APERTURE)	94.54	.000	.000
PATH PARAMETERS			
SPACE LOSS (R=46720. KM).....	-274.87	.000	.000
RECEIVER PARAMETERS			
IDEAL APERTURE GAIN(.261M APERTURE)	97.77	.000	.000
OBSCURATION LOSS (GAMMA=.200).....	-.18	.000	.000
IMAGE MOTION COMPENSATOR LOSS.....	-.46	.048	-.049
LOCAL OSCILLATOR DIPLEXER LOSS.....	-.04	.004	-.004
BEACON DIPLEXER LOSS.....	-.13	.013	-.013
OPTICS REFLECTANCE LOSSES.....	-.44	.086	-.092
HETERODYNE DETECTION LOSS.....	-1.85	.225	-.237
DETECTOR NOISE DEGRADATION.....	-.47	.084	-.208
PLANCK'S CONSTANT.....	331.78	.000	.000
CARRIER FREQUENCY,DB(HZ).....	-134.52	.000	.000
DETECTOR QUANTUM EFFICTENCY.....	-2.22	.000	-.792
IF BANDWIDTH,DB(HZ) (704.MHZ).....	-88.48	.000	.000
	--------	--------	--------
IF SIGNAL TO NOISE RATIO.....	15.89	.666	-1.680

50039-1(U)

FIGURE 2-1. LDRL-10.6 EXPERIMENT LINK DESIGN CONTROL TABLE

A detector noise degradation factor defined by

$$\eta_N = \frac{(S/N)_{IF}}{(S/N)_{IF_{ideal}}} \tag{2-3}$$

accounts for the degradation from ideal performance due to all noise mechanisms. The $(S/N)_{IF}$ may then be written in the more compact form

$$(S/N)_{IF} = \frac{P_s \eta \eta_N}{h\nu_c B_{IF}} \tag{2-4}$$

which facilitates representation in dB form. The received signal power at the detector is given by*

$$P_s = P_T \eta_T G_T \eta_S G_R \eta_R \tag{2-5}$$

where

P_T = modulated laser output power

η_T = transmitter loss

G_T = transmitter aperture gain

η_S = space loss

G_R = receiver aperture gain

η_R = receiver loss

Substituting this expression into Equation 2-4 gives

$$(S/N)_{IF} = \frac{P_T \eta_T G_T \eta_S G_R \eta_R \eta \eta_N}{h\nu_c B_{IF}} \tag{2-6}$$

The LDR L-10.6 Design Control Table (DCT) of Figure 2-1 expresses Equation 2-6 in logarithmic (dB) form. The losses are itemized in detail with respect to

*Equation 2-5 neglects atmospheric losses since a space to space link (shuttle to Molniya) is assumed.

specific system elements. The DCT is a dB summation of power, gains, and losses that determine $(S/N)_{IF}$ for a specified link. Figure 2-1 is a DCT for the most critical LDRL-10.6 situation: a 400 Mbps low earth orbit shuttle to Molniya link (maximum range, 46.720 km). The indicated $(S/N)_{IF}$ of 15.89 dB allows for a 6 dB margin with a bit error probability, $P_e = 10^{-6}$. The 0.18 meter transmitter aperture is specified; the receiver aperture diameter and transmitted power are then optimized for minimum system weight. Each DCT entry is defined and its evaluation discussed in the following paragraphs.

2.1.1 Transmitter Parameters

Modulated Laser Output Power

The modulated laser output power is the modulated sideband power into the transmitter optical system. Laser power may be specified as an input, determined by other specified inputs, or optimized for minimum system weight.

Beam Expander Loss

The beam expander loss is due to attenuation and reflection losses by the two element Zinc Selenide beam pre-expander optics (Figure 4-11). Attenuation for ZnSn is 0.01 percent per cm; reflectance is 0.999 per surface. There are six surfaces since one element is a doublet. The net beam expander loss is 0.986.

Diplexer Loss

The transmitter diplexer (beam splitter) (Figure 4-11) reflects the incoming beacon signal to its receiver (during the acquisition phase) while transmitting the outgoing communication signal. The diplexer consists of a wire-grid polarizer and a quarter wave plate. The cominbation has a net loss of approximately 0.91.

Image Motion Compensator Loss

The transmitter IMC loss is due to reflectance of 0.975 at each of the two gold electroplated IMC mirror surfaces. The resultant IMC loss is $(0.975)^2 = 0.951$.

Optics Reflectance Loss

The optics reflectance is approximately 0.975 at each of the six gold electroplated reflecting elements in the transmitter optical system. These are as follows:

1) Inner gimbal pointing mirror

2) Large folding mirror

3) Primary paraboloid

4) Secondary paraboloid

5) Small folding mirror

6) Relay mirror

The net loss due to these six elements is then $(0.975)^6 = 0.859$.

Obscuration Loss

The transmitter obscuration loss accounts for the reduced far field axial gain of a Gaussian illuminated and obscured circular aperture relative to a uniformly illuminated and unobscured one. The relative degradation is given by (Reference 1)

$$g_T = \frac{2}{\alpha^2}\left[e^{-\alpha^2} - e^{-\alpha^2\gamma_T^2}\right]^2 \qquad (2\text{-}7)$$

where

γ_T is the transmitter optics diameter obscuration ratio. γ_T is a function of the aperture diameter, D_T

α is the laser beam truncation defined as the ratio of beam width (in the obscuration plane) to primary aperture diameter.

The obscuration loss is calculated by the Link Analysis Program using the γ_T (D_T) required for the 1° acquisition field of view and f/1.5 transmitter optics. The optimum value of α for a Gaussian laser beam intensity distribution is used, approximated by

$$\alpha = 1.12 - 1.30\,\gamma_T^2 + 2.12\,\gamma_T^4 \qquad (2\text{-}8)$$

Figure 2-2 depicts g_T, dB as a function of γ_T for $\alpha = \alpha_o$.

For the 0.18 meter aperture LDRL-10.6 system, $\gamma = 0.412$ and the obscuration loss is

$$g_T = 0.454 \text{ (or } -3.43 \text{ dB)} \qquad (2\text{-}9)$$

Pointing Loss

Pointing loss results from the receiver being displaced from the maximum of the transmitter far-field gain pattern due to pointing error. The nominal pointing loss is zero since it is intended that point-ahead angle be corrected entirely. However, even if point-ahead angle information were known with absolute accuracy, it is estimated that pointing error would be of the order of 5 μrad. For the far field gain pattern corresponding to the aperture diameter obscuration $\gamma_T = 0.412$ (0.18 meter transmitter aperture), this represents a gain loss of 0.982 (-0.079 dB) compared to the maximum (axial) gain.

Ideal Aperture Gain

The ideal aperture gain is the maximum axial far field gain (relative to an isotropic radiator) achievable with a uniformly illuminated, unobscured circular aperture

$$G_T = \left(\frac{\pi D_T}{\lambda}\right)^2 \tag{2-10}$$

where λ is the wavelength and D_T is the transmitter aperture diameter.

2.1.2 Path Parameters

Space Loss

Space loss is given by

$$\eta_S = \left(\frac{\lambda}{4\pi R}\right)^2 \tag{2-11}$$

where λ is the wavelength and R is the communication range.

2.1.3 Receiver Parameters

Ideal Aperture Gain

The ideal gain for a uniformly illuminated, unobscured circular aperture of diameter D_R is

$$G_R = \left(\frac{\pi D_R}{\lambda}\right)^2 \tag{2-12}$$

Obscuration Loss

Obscuration of the receiver aperture affects performance most directly by reducing the effective area of the receiver aperture.

In terms of the receiver diameter obscuration ratio γ, the receiver obscuration loss is the ratio of the obscured to unobscured aperture areas given by

$$g_R = (1 - \gamma^2) \tag{2-13}$$

Receiver obscuration loss, g_R, dB versus γ is plotted in Figure 2-3. Obscuration of the receiver aperture causes an additional loss by degrading the efficiency of the heterodyne detection process. This effect is included in the heterodyne detection loss. For the LDRL-10.6 receiver, $\gamma = 0.2$, and the obscuration loss is given by $g_R = 0.96$.

Image Motion Compensator Loss

The receiver image motion compensator loss is due to a 0.975 reflectance at each of the two gold electroplated IMC mirrors and the nutation loss attendant to generating the IMC error signal. The receiver IMC net loss is approximately 0.90.

Local Oscillator Diplexer Loss

The local oscillator diplexer loss is primarily due to imperfect reflection since the incoming beam is not transmitted by the diplexer. The local oscillator diplexer loss is approximately 0.99.

Beacon Diplexer Loss

Beacon diplexer loss is due to both transmission and reflection of the incoming beam. The net beacon diplexer loss is approximately 0.97.

Optics Reflectance Losses

Optics reflectance loss is approximately 0.975 at each of the four gold electroplated reflecting elements in receiver optical system. These are as follows:

1) Pointing mirror

2) Primary paraboloid

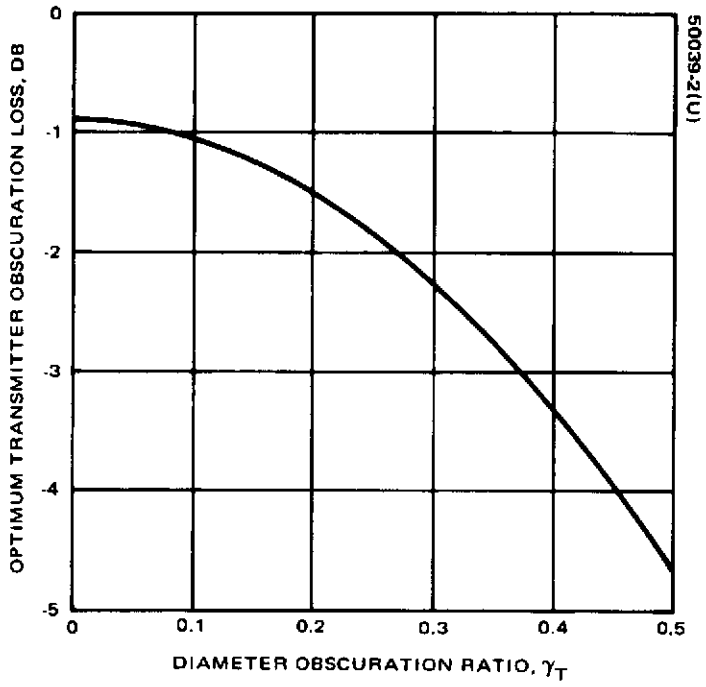

FIGURE 2-2. AXIAL GAIN OF OPTIMUM GAUSSIAN ANTENNA RELATIVE TO $\left(\frac{\pi D_T}{\lambda}\right)^2$ AS FUNCTION OF OBSCURATION RATIO γ_T

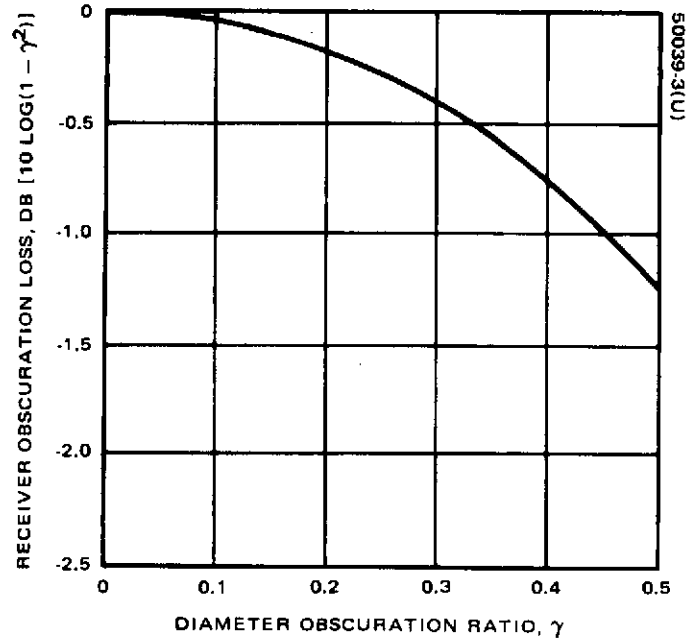

FIGURE 2-3. RECEIVER LOSS IN DB DUE TO CENTRAL OBSCURATION

3) Secondary paraboloid

4) Folding mirror

The loss of the four elements is then $(0.975)^4 = 0.904$.

Heterodyne Detection Loss

The heterodyne detection loss depends on the electric field distributions of the signal and local oscillator on the detector. For the readily implemented case of a uniform local oscillator field distribution, the heterodyne detection loss is given by (Reference 2)

$$\eta_H = \left[4/(1-\gamma^2)\right]\left\{\left[J_o(\gamma\,\sigma r) - J_o(\sigma r)\right]/\sigma r\right\}^2 \qquad (2\text{-}14)$$

where

γ = receiver optics diameter obscuration ratio

$\sigma = k R_A/2F_S$

$k = 2\pi/\lambda$

R_A = Airy disk size

F_S = system f number

$r = R_D/R_A$

R_D = detector radius

η_H is plotted in Figure 2-4 (Reference 2) as a function of R_D/R_A with γ as a parameter. It is evident from Figure 2-4 that η_H is a maximum for $R_D/R_A \approx 0.75$. This optimum detector size minimizes the $(S/N)_{IF}$ degradation due to local oscillator generated detector shot noise. For the LDRL-10.6 receiver, $\gamma = 0.2$ so that for $R_D/R_A = 0.75$, $\eta_H = 0.653$.

Detector Noise Degradation

As discussed previously, detector noise degradation η_N is an artifice to compactly account for all detector noise mechanisms

$$\eta_N = \frac{(S/N)_{IF}}{(S/N)_{IF_{ideal}}} \qquad (2\text{-}15)$$

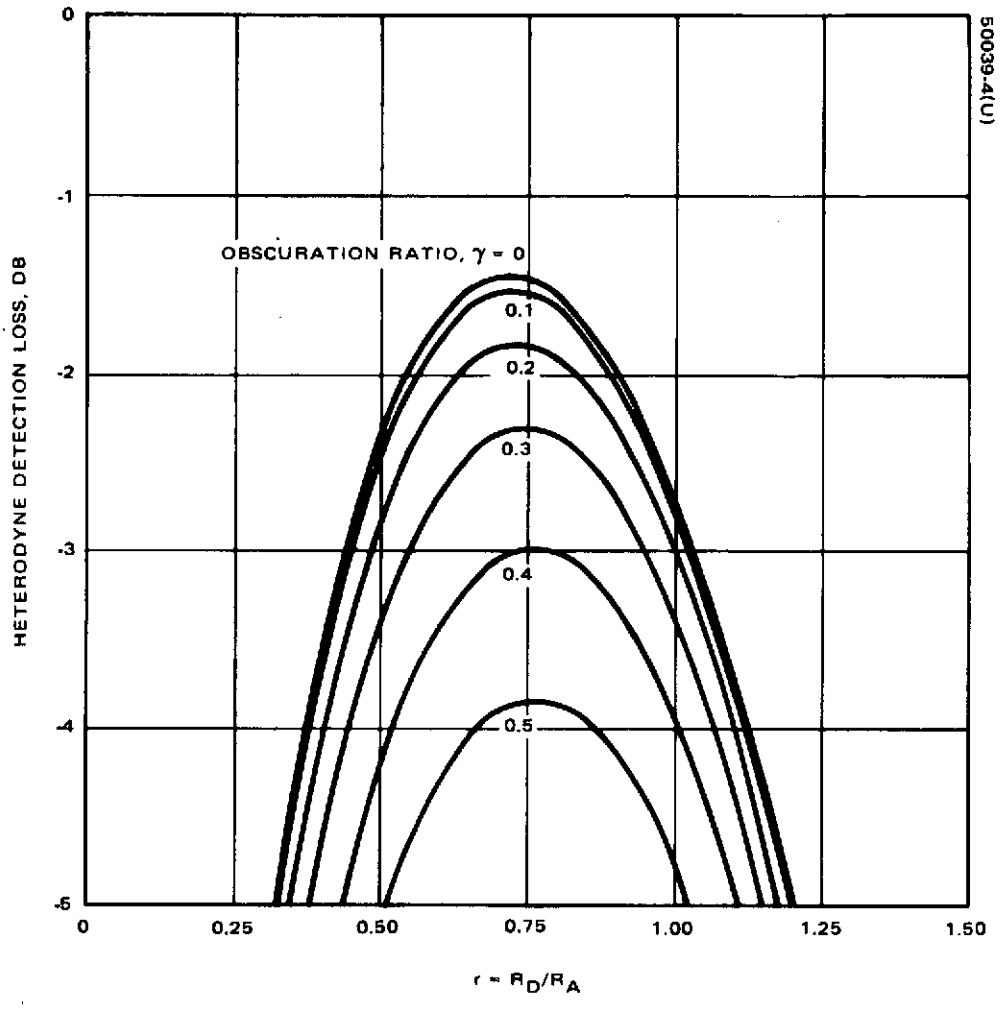

FIGURE 2-4. HETERODYNE DETECTION LOSS FOR UNIFORM LOCAL OSCILLATOR INTENSITY DISTRIBUTION AS FUNCTION OF DIAMETER OBSCURATION RATIO γ AND RATIO OF DETECTOR RADIUS TO AIRY SPOT RADIUS

where $(S/N)_{IF_{ideal}}$ results from the dominant local oscillator noise case (all other noise sources negligible). η_N is calculated in the Link Analysis Program.

Planck's Constant

Planck's constant relates photon energy to photon (carrier) frequency:

$$h \approx 6.625 \times 10^{-34} \text{ J} \cdot \text{sec} \tag{2-16}$$

Carrier Frequency

The carrier frequency corresponding to the 10.6 micrometer wavelength is

$$\nu_c \approx 2.82823 \times 10^{13} \text{ Hz} \tag{2-17}$$

Detector Quantum Efficiency

Quantum efficiency is the detector conversion efficiency between light and electrical energy. A quantum efficiency of 0.50 is readily realizable; 0.60 appears feasible.

IF Bandwidth

The system IF bandwidth (B_{IF}) requirement is a function of the link data rate (R_b). The signaling (low pass) bandwidth (B_o) corresponding to B_{IF} is $B_o = B_{IF}/2$. For a given detection method, the detector performance degradation from the ideal matched filter case due to thermal noise and intersymbol interference depends on the ratio B_o/R_b. The relationship between B_o/R_b and detector performance degradation has been examined for a number of detection methods (Reference 3). One readily implemented (hence, attractive) detection scheme for binary digital data uses the "band limit and sample" detector. For this situation, the detector performance degradation may be minimized by the optimal choice of B_o/R_b. The detector performance degradation may be characterized by the increase in P_e (for constant bit energy/spectral noise density, E_b/N_o) or, alternatively, by the increase in E_b/N_o required to maintain a constant P_e. Figure 2-5 depicts $\Delta E_b/N_o$ (for constant P_e) as a function of B_o/R_b. Note that for the

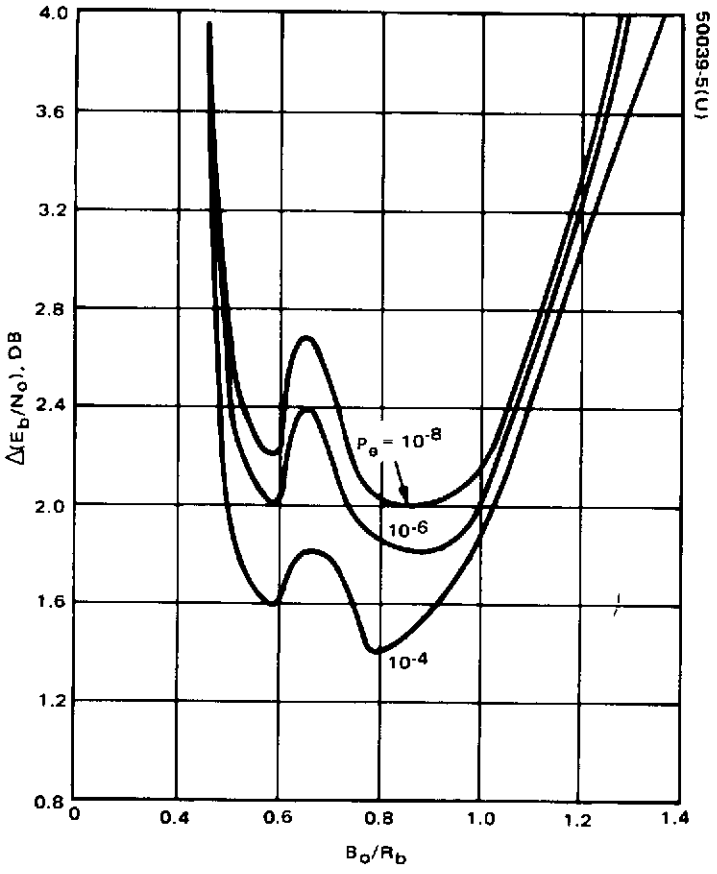

FIGURE 2-5. $\Delta(E_b/N_o)$ VERSUS B_o/R_b FOR BAND LIMIT AND SAMPLE DETECTION

LDRL-10.6 requirement of $P_e = 10^{-6}$, the detector performance degradation is minimized for $B_o/R_b \approx 0.88$. The corresponding required IF bandwidth for the LDRL 400 x 10^6 bps data rate is then

$$B_{IF} = 2\,B_o$$

$$= 2 \times 0.88 \times R_b \qquad (2\text{-}18)$$

$$= 704 \times 10^6 \text{ Hz}$$

Intermediate Frequency Bandwidth Signal-to-Noise Ratio

The required $(S/N)_{IF}$ to detect with specified P_e depends on the detection method used. For the chosen band limit and sample scheme, required $(S/N)_{IF}$ is determined by (B_o/R_b). Figure 2-6 (Reference 3) depicts P_e as a function of E_b/N_o with B_o/R_b as a parameter. For $P_e = 10^{-6}$ and the corresponding optimum value of $B_o/R_b \approx 0.88$, the E_b/N_o required is approximately 17.159 (12.345 dB). The $(S/N)_{IF}$ is then determined,

$$(S/N)_{IF} = \left(\frac{E_b}{N_o}\right) / \left(\frac{B_{IF}}{R_b}\right) \qquad (2\text{-}19)$$

$$= 9.749 \text{ or } 9.89 \text{ dB} \qquad (2\text{-}20)$$

An additional 6 dB margin is included to accommodate design uncertainties. The resultant $(S/N)_{IF} = 15.89$ dB has been used as a basis for the LDRL system preliminary performance calculations summarized in Figure 2-1 and the revised weight optimization (see subsection 2.4).

2.2 LINK ANALYSIS PROGRAM TOLERANCE ANALYSES

In addition to the calculation of LDRL $(S/N)_{IF}$ (or optimizations for specified $(S/N)_{IF}$) for nominal link parameter values, the Link Analysis Program also performs parallel calculations for favorable and adverse values of all link parameters and displays the corresponding tolerances about each nominal entry in the Design Control Table, as indicated in Figure 2-1. The resultant display facilitates the evaluation of link performance sensitivity to variation in critical parameters. The present input tolerance values indicated in the Link Analysis Program tabulation of link parameters (Figure 2-7) are preliminary.

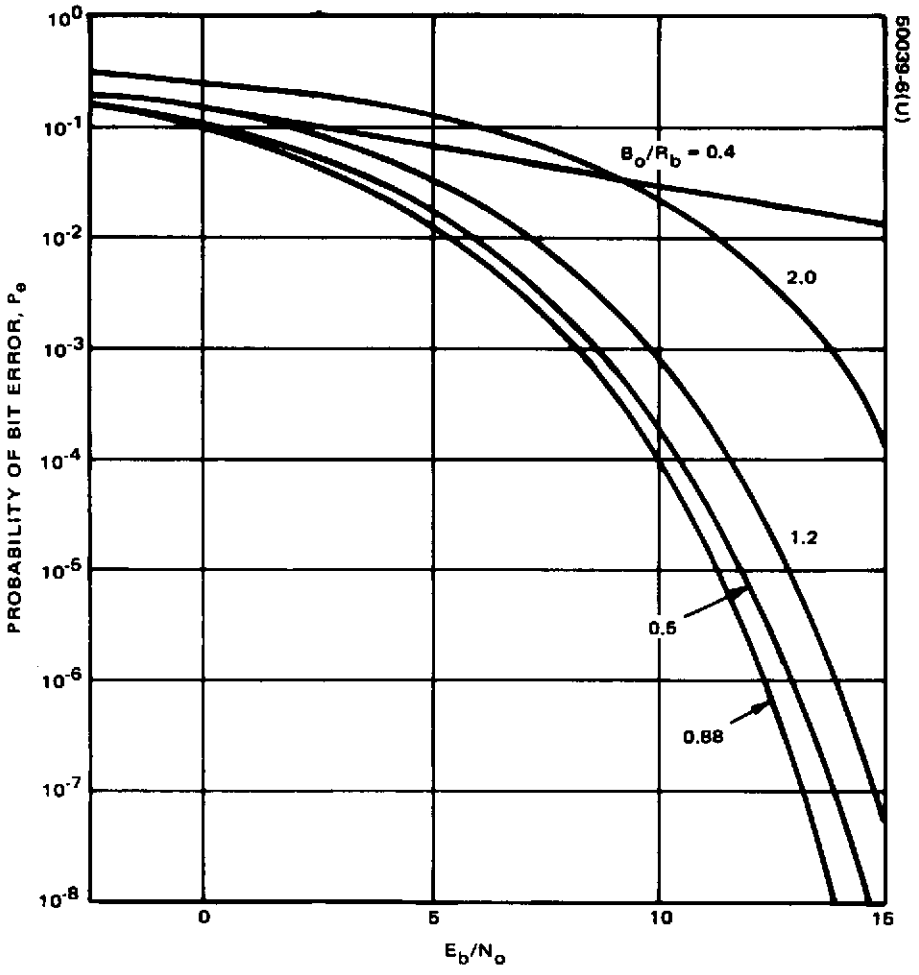

FIGURE 2-6. P_e VERSUS E_b/N_o FOR BAND LIMIT AND SAMPLE DETECTION

CONSTANTS USED IN LDRL LINK BUDGET CALCULATIONS

	NOMINAL	FAV. TOL.	ADV. TOL.
TRANSMITTER PARAMETERS			
MODULATED LASER OUTPUT POWER,DBM(W)	1.05	.00	.00
BEAM EXPANDER LOSS,PERCENT	1.40	-.14	.14
DIPLEXER LOSS,PERCENT	9.00	-.90	.90
IMAGE MOTION COMPENSATOR LOSS,PERCENT	4.90	-.49	.49
OPTICS REFLECTANCE LOSSES,PERCENT	10.10	-2.70	2.60
POINTING ERROR,MICRORADIANS	.00	.00	-5.00
POINTING LOSS,PERCENT	.00	.00	1.60
RECEIVER PARAMETERS			
IMAGE MOTION COMPENSATOR LOSS,PERCENT	10.00	-1.00	1.00
LOCAL OSCILATOR DIPLEXER LOSS,PERCENT	1.00	-.10	.10
BEACON DIPLEXER LOSS,PERCENT	3.00	-.30	.30
OPTICS REFLECTANCE LOSSES,PERCENT	9.60	-1.80	1.40
HETERODYNE DETECTION LOSS,PERCENT	34.70	-5.47	3.47
DETECTOR QUANTUM EFFICIENCY,PERCENT	60.00	.00	-10.00
DETECTOR GAIN	1.00	.00	.00
DETECTOR LOAD RESISTANCE,OHMS	50.00	.00	.00
DETECTOR DARK CURRENT,MICROAMPS	.100000	-.010000	.010000
POSTAMPLIFIER NOISE TEMPERATURE,DEGREES K	350.00	-35.00	35.00
LOCAL OSCILLATOR POWER,WATTS	.002000	-.000200	.000200
BACKGROUND RADIANCE,WATTS/SQ M*MICRONS*STERADIAN	.001000	-.000100	.000100
DETECTOR FIELD OF VIEW,MICRORADIANS	56.02	.00	.00

50039-7(U)

FIGURE 2-7. CONSTANTS USED IN LDRL LINK BUDGET CALCULATIONS

2.3 TRANSMITTER APERTURE OBSCURATION VERSUS DIAMETER

Required transmitter aperture diameter obscuration ratio, γ_T, (to maintain the 1° FOV of the f/1.5 transmitter optics) increases rapidly with aperture diameter. The resultant obscuration loss degrades the net aperture gain with increasing severity (Figure 2-2). This implied relationship between transmitter aperture diameter and obscuration loss must be taken into consideration in determining the optimum aperture diameter. As increasingly larger apertures become relatively less gainful due to increasing obscuration loss, the effect is to shift the optimum aperture diameter toward smaller values. The dependence of obscuration on aperture diameter for the f/1.5, 1° FOV LDRL transmitter optics is depicted in Figure 2-8. The curve of Figure 2-8 is an empirical fit to data obtained by ray traces for several f/1.5, 1° FOV systems. The empirical expression obtained is

$$\gamma_T = 0.3542 + 18.8369\, D_T^{3.3746} \qquad (2\text{-}21)$$

where D_T is the transmitter aperture diameter in meters.

A similar model is appropriate to receiver obscuration dependence on aperture diameter. The receiver obscuration may be expected to be smaller than that of the transmitter (for similar f number and aperture), since the receiver terminal vehicle is assumed to be unmanned (hence, with improved attitude stability and a correspondingly smaller receiver FOV requirement). However, the aperture diameter optimization depends on the derivative of obscuration loss with respect to diameter rather than the loss itself. Furthermore, the effect of aperture diameter (hence, obscuration) variation on the heterodyne detection efficiency must be considered in addition to the area obscuration loss. Thus the counterpart receiver problem is somewhat more complex. Since optimization of the detailed receiver characteristics is not considered within the scope of the LDRL program, the receiver obscuration ratio has been assumed constant. The receiver obscuration value of $\gamma = 0.2$ used in the Link Analysis Program corresponds to the 0.26° FOV receiver of the Opto Mechanical Subsystem of a 10.6 Micrometer Wavelength Receiver Terminal Program (Contract NAS 5-21859).

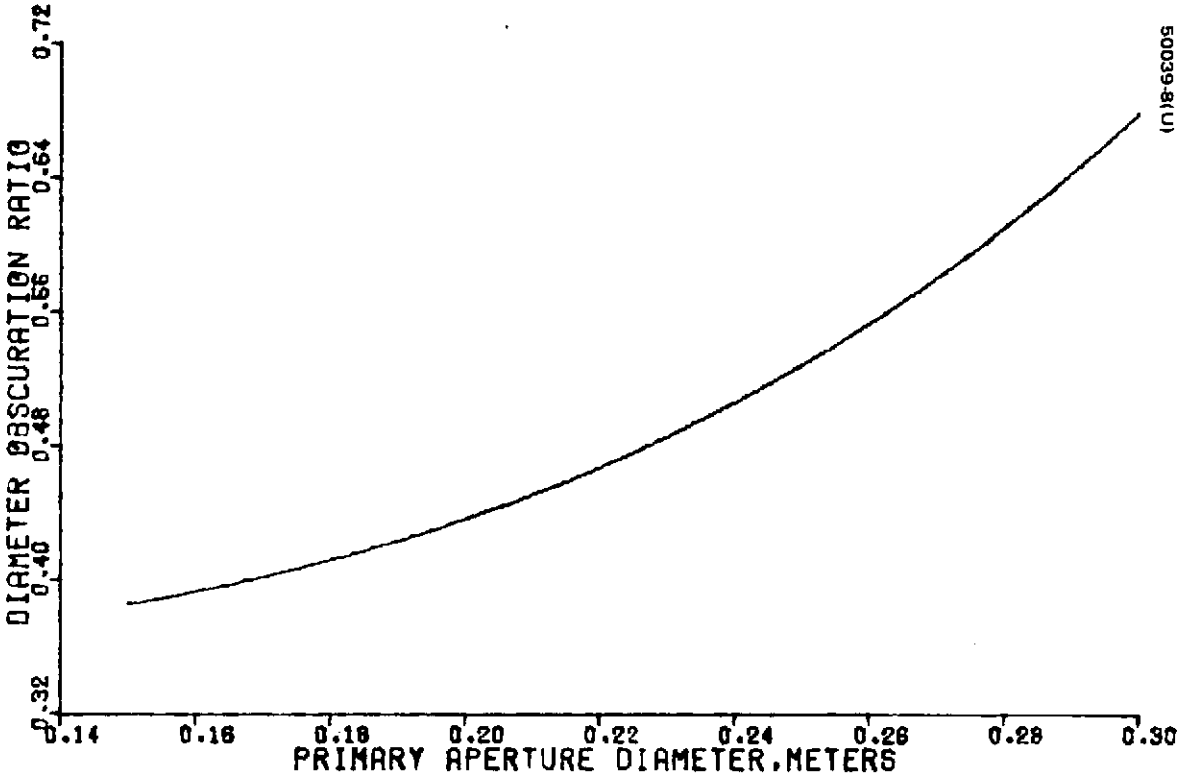

FIGURE 2-8. LDRL TRANSMITTER APERTURE OBSCURATION RATIO VERSUS DIAMETER FOR f NUMBER = 1.5 AND FOV = 1^{o}

2.4 REVISED LDRL WEIGHT OPTIMIZATION

The LDRL system weight optimization (Link Analysis Program) has been revised to take into account the following:

1) Refined assessment of IF bandwidth and signal-to-noise ratio required to meet the specified LDRL 400 Mbps data rate with $P_e = 10^{-6}$ and a 6 dB margin

2) Refined evaluation and modeling of LDRL system losses

3) Modeling of transmitter aperture obscuration (and obscuration loss) as a function of aperture diameter

The revised LDRL weight optimization and weight budget results for the 46, 720 km range, 400 Mbps (and chosen 0.18 meter transmitter aperture) LDRL are presented in Figure 2-9. Figure 2-9 is for the most critical LDRL mission and corresponds to the LDRL Design Control Table of Figure 2-1. For the LDRL system of Figures 2-9 (and 2-1), a transmitter aperture diameter of 0.18 meter was specified, and transmitter power and receiver aperture were optimized for minimum total system weight. The methodology of the weight optimization (Link Analysis) program and the system weight modeling details were presented in the first quarterly report. (Reference 4).

2.5 LDRL WEIGHT OPTIMIZATION SENSITIVITY

Sensitivity of LDRL transmitter package associated (including power supply) weight to transmitter aperture diameter variations about the optimum (minimum system weight point) has been investigated as a guide to system weight/cost tradeoffs. For the 46,720 km range, 400 Mbps LDRL, Figure 2-10 depicts transmitter package associated weight as a function of transmitter aperture diameter, with transmitter power and receiver aperture diameter optimized for minimum system (transmitter and receiver packages) weight at each point. Figure 2-10 clearly shows that system weight is relatively insensitive to transmitter aperture diameter variations over a range of several centimeters about the optimum point. Reduction in transmitter aperture diameter at a small weight penalty is thus encouraged if system cost can be reduced thereby (as long as the saving in aperture cost is not negated by that of the requisite transmitter power increase). It was this compromise between system weight and cost that led to the chosen 0.18 meter transmitter aperture diameter.

IF BANDWITH,MHZ 704.

OPTIMIZED VALUES

PACKAGE B (TRANSMITTER) ANTENNA DIAMETER,M	.1800
PACKAGE A (RECEIVER) ANTENNA DIAMETER,M	.2611
TRANSMITTER OUTPUT POWER,WATTS	1.0536
TRANSMITTER EFFICIENCY,PERCENT	1.0173

PACKAGE B WEIGHT TABULATION,POUNDS

STRUCTURE WEIGHT	24.37
OPTICAL TELESCOPE WITH MOUNTINGS	8.15
GIMBALS,MOTORS,AND STEERING MIRROR	9.72
SERVO ELECTRONICS	4.42
LASER,MODULATOR,AND MODULATOR DRIVER (1)	26.03
SERVO POWER CONDITIONING	7.33
OTHER POWER CONDITIONING	12.50
DIPLEXER AND MISCELLANEOUS OPTICS	3.06
LASER STABILIZATION ELECTRONICS	.40
BEACON DETECTOR AND POWER SUPPLY (1)	.58
BEACON RECEIVER OPTICS AND ELECTRONICS	.66
IMAGE MOTION COMPENSATION SUBSYSTEM	2.62
CABLES AND CONNECTORS	1.71
MISCELLANEOUS	10.16
PACKAGE B TOTAL WEIGHT	111.71
ASSOCIATED PRIME POWER SYSTEM WEIGHT	118.54
PACKAGE B ASSOCIATED WEIGHT BURDEN	230.24

PACKAGE B POWER TABULATION WATTS

TRANSMITTER LASER INPUT POWER	103.57
TRANSMITTER ELECTRONICS POWER	76.00
POINTING SUBSYSTEM POWER	8.25
BEACON RECEIVER POWER	1.00
CONTROL PANEL POWER	10.00
PACKAGE B SYSTEM POWER	198.82

PACKAGE A WEIGHT TABULATION,POUNDS

STRUCTURE WEIGHT	22.81
OPTICAL TELESCOPE WITH MOUNTINGS	14.72
GIMBALS,MOTORS,AND STEERING MIRROR	11.63
SERVO ELECTRONICS	4.06
RECEIVER AND SIGNAL PROCESSING ELECTRONICS (1)	20.10
SERVO POWER CONDITIONING	8.11
OTHER POWER CONDITIONING	12.00
BEACON LASER (1)	3.00
LOCAL OSCILLATOR LASER (1)	2.00
DETECTOR AND DETECTOR COOLER	3.50
BEAM EXPANDER AND DEFOCUS MECHANISM	8.70
IMAGE MOTION COMPENSATION SUBSYSTEM	4.17
CABLES AND CONNECTORS	2.53
MISCELLANEOUS	11.73
PACKAGE A TOTAL WEIGHT	129.05
ASSOCIATED PRIME POWER SYSTEM WEIGHT	96.92
PACKAGE A ASSOCIATED WEIGHT BURDEN	225.97

PACKAGE A POWER TABULATION WATTS

LOCAL OSCILLATOR INPUT POWER	13.00
RECEIVER ELECTRONICS POWER	26.28
POINTING SUBSYSTEM POWER	9.95
BEACON TRANSMITTER POWER	100.00
CONTROL PANEL POWER	10.00
PACKAGE A SYSTEM POWER	159.23

FIGURE 2-9. LINK PARAMETERS FOR 400 MBPS DESIGN

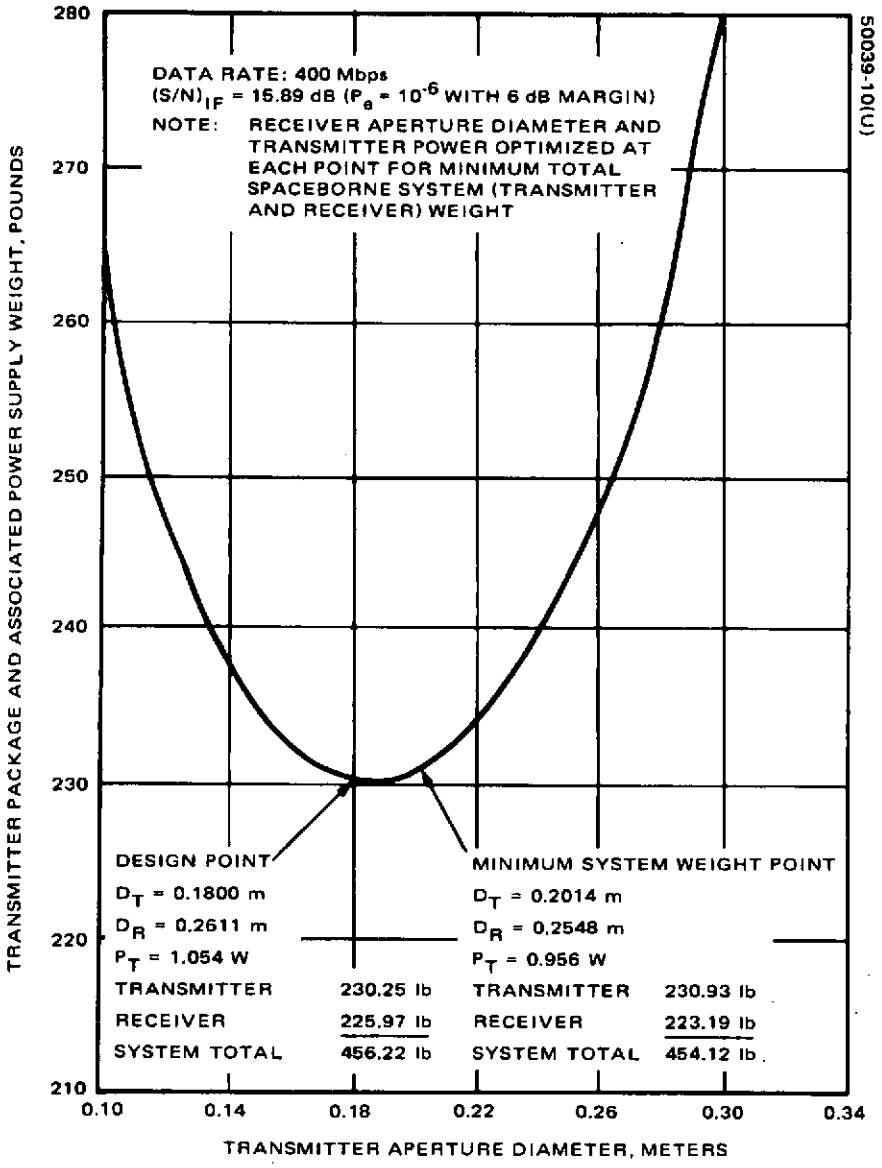

FIGURE 2-10. LDRL TRANSMITTER ASSOCIATED WEIGHT VERSUS TRANSMITTER APERTURE DIAMETER (RANGE = 46,720 KM)

3. LINK ESTABLISHMENT

The link establishment problem has two phases: acquisition and tracking. Two links are to be established: the shuttle to Molniya and the shuttle to ground. The shuttle terminal is a communication transmitter with a beacon receiver, while the Molniya (or ground) terminal is a communication receiver with a beacon transmitter. Savings in weight, as well as cost and complexity, favor utilizing the 10.6 μm wavelength for link establishment, maintenance, and communication.

The shuttle to ground link has a signal-to-noise advantage due to the proximity of the terminals (in comparison to the shuttle to Molniya link). This proximity, however, imposes very high angular rates and diminishes the time available for link establishment. Moreover, atmospheric propagation effects are present in this link and should be considered. For these reasons, the shuttle to ground link is considerably more difficult to establish. In the following paragraphs, both links are examined. The shuttle to ground link discussion deals primarily with definition of an acquisition concept that alleviates the image motion compensation requirements (see 5.2). With these guidelines, the following acquisition concept was chosen for further investigation.

3.1 SHUTTLE TO MOLNIYA LINK

The shuttle initiates the acquisition phase by illuminating the uncertainty cone (cone angle $\theta_{I\ell} \simeq 1°$) while simultaneously scanning the same uncertainty cone with its narrowbeam (θ_{br}, ~60 μrad) beacon receiver. The receiver on the Molniya spacecraft scans its own uncertainty cone (cone angle $\theta_s \simeq 0.5°$) with its narrow beam, θ_r, until it locates the shuttle transmitter. Then the tracking phase is initiated and the beacon is turned on illuminating the shuttle by reciprocity. This beacon has same beamwidth as the receiver ($\theta_{bt} = \theta_r$ ~42 μrad) and coaxial with the communication receiver. The shuttle continues scanning with its narrowbeam ($\theta_{br} = \theta_t$) beacon receiver until it detects the Molniya beacon. At this instant, the tracking mode of the shuttle beacon receiver starts. The transmitter is turned to the narrowbeam (θ_t) communications mode with the appropriate lead angle applied to the beacon receiver path.

3.1.1 Acquisition Signal-to-Noise Ratio (Molniya Acquires Shuttle)

The link performance during acquisition (Reference 5) illustrated in Figure 3-1 depends on the illumination cone angle

$$(SNR)_A = (SNR)_{IF}\left(\frac{\theta_t}{\theta_{I\ell}}\right)^2 L_A \tag{3-1}$$

where $(SNR)_{IF}$ is the signal-to-noise ratio in the IF in the communications mode, θ_t the shuttle transmitter beamwidth, $\theta_{I\ell}$ the illumination cone angle (beamwidth), and L_A the additional loss (gain) of the acquisition transfer optics in the transmitter.

3.1.2 Mean Time to Acquire

The acquisition time (Reference 5) is at most

$$T_m = \left(\frac{\theta_s}{\theta_r}\right)^2 \frac{k}{B_a} \tag{3-2}$$

where θ_s is the search cone angle of the receiver on the Molniya satellite, θ_r its beamwidth, $k/B_a \triangleq \tau$ the dwell time per resolution element, B_a the acquisition baseband, and k a factor depending on rise time and field scan logic. This, of course, assumes that the probability of detection when the target is present somewhere in the uncertainty cone is unity ($P_d = 1$). The average time to acquisition under this condition is

$$T = \frac{1}{2}T_m = \frac{k}{2B_a}\left(\frac{\theta_s}{\theta_r}\right)^2 \tag{3-3}$$

When the detection probability is $P_d < 1$, the average acquisition time is longer because one must provide for the case where the target is missed (the probability of this is $1 - P_d$). Of course, there is also a false alarm probability, Q_o, of detecting a target when none exists.

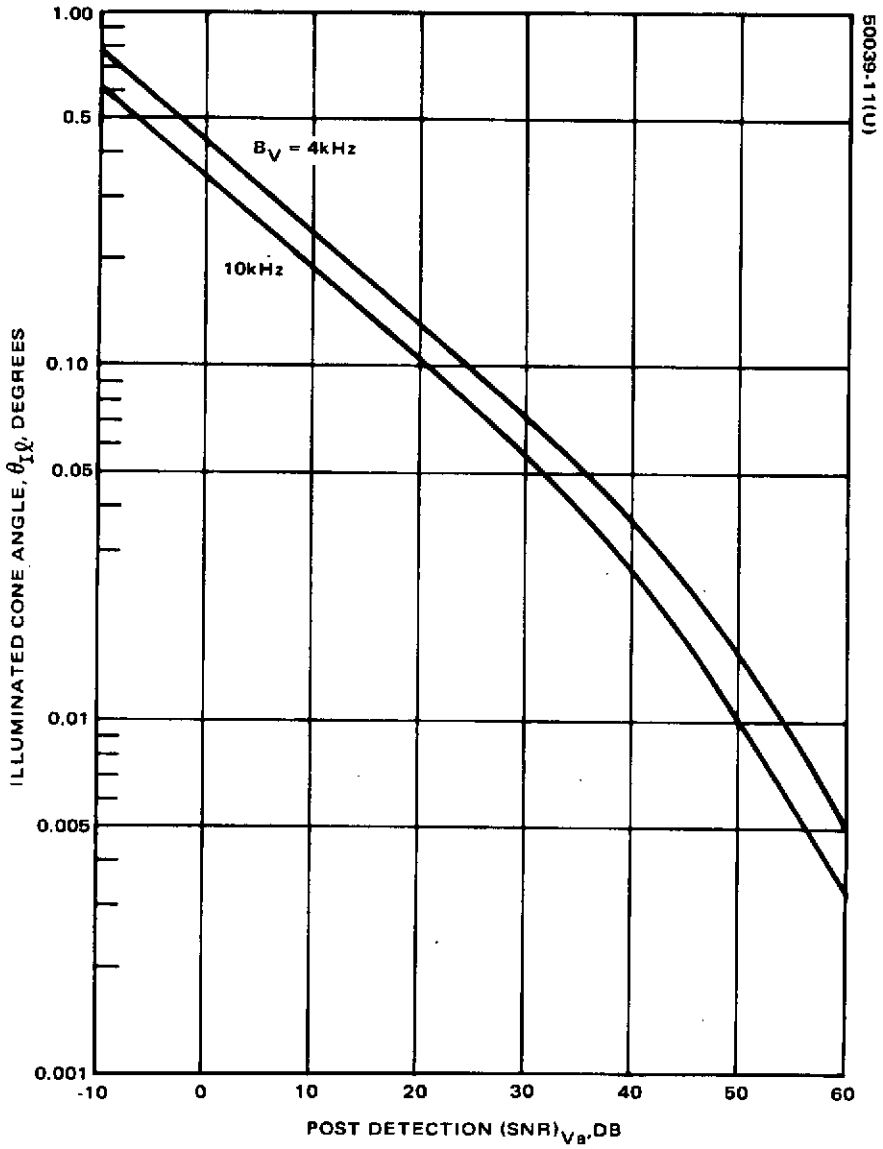

FIGURE 3-1. ILLUMINATED CONE ANGLE VERSUS POSTDETECTION $(SNR)_{Va}$

Let T_ℓ be the time lost due to acquiring a false target. Now the average lost time per frame will be

$$\bar{T}_L = Q_o T_\ell \left[\left(\frac{\theta_s}{\theta_r}\right)^2 - 1\right] \tau \tag{3-4}$$

Consequently, the average time to scan a frame without a target being present is

$$T = \left(\frac{\theta_s}{\theta_r}\right)^2 \tau + \bar{T}_L = \left[\left(\frac{\theta_s}{\theta_r}\right)^2 1 + Q_o T_\ell \quad - Q_o T_\ell\right] \tau \tag{3-5}$$

Assume now that the target is definitely within the uncertainty cone (frame). Then, on the average, it will take

$$E[T_1] = \frac{T}{2} P_d \tag{3-6}$$

to detect the target in the first frame scan.

The expected time to detect the target in the second scan is

$$E[T_2] = (P_d - 1)P_d T + (1 - P_d)P_d \frac{T}{2} = \frac{3}{2} T P_d (1 - P_d) \tag{3-7}$$

where the first term represents the time wasted in the first scan weighted by the probability of finding the target in the second scan, and the second term represents the average time to find the target in the second scan given that it was not detected in the first scan.

Similarly, the expected time to find the target in the m^{th} scan is

$$E[T_m] = (1 - P_d)^{m-1} P_d T + (1 - P_d)^{m-1} P_d \frac{T}{2}$$

$$= \frac{2m + 1}{2} T P_d (1 - P_d)^{m-1} \tag{3-8}$$

Therefore, the average time to acquisition is

$$T_a = \frac{1}{2}TP_d + \frac{3}{2}TP_d(1 - P_d) + \frac{5}{2}TP_d(1 - P_d)^2 + \ldots \quad (3\text{-}9)$$

Performing the sum results finally in

$$T_a = \frac{T}{2}\left(\frac{2 - P_d}{P_d}\right) \quad (3\text{-}10)$$

which after substitution of T from Equation 3-5 yields

$$T_a = \frac{k}{2B_a}\left\{\left(\frac{\theta_s}{\theta_r}\right)^2 [1 + Q_o T_\ell] - Q_o T_\ell\right\}\left(\frac{2 - P_d}{P_d}\right) \quad (3\text{-}11)$$

This is a function of the postdetection $(SNR)_{Va}$ at the Molniya receiver because the $(SNR)_{Va}$ determines the P_d after a certain probability of false alarm, Q_o, has been specified.

Observe that Equation 3-11 reduces to Equation 3-3 under the conditions

$$Q_o = 0, \quad P_d = 1 \quad (3\text{-}12)$$

Equation 3-11 is plotted in Figure 3-2, as a function of $(SNR)_{Va}$.

Equation 3-11 gives the average time to acquire the shuttle. The shuttle starts its acquisition after being illuminated by the Molniya beacon. The average time to acquire the Molniya is

$$T_A = \frac{k}{2B_A}\left\{\left(\frac{\theta_n}{\theta_t}\right)^2 [1 + Q_1 T_\ell] - Q_1 T_\ell\right\}\left(\frac{2 - P_D}{P_D}\right) \quad (3\text{-}13)$$

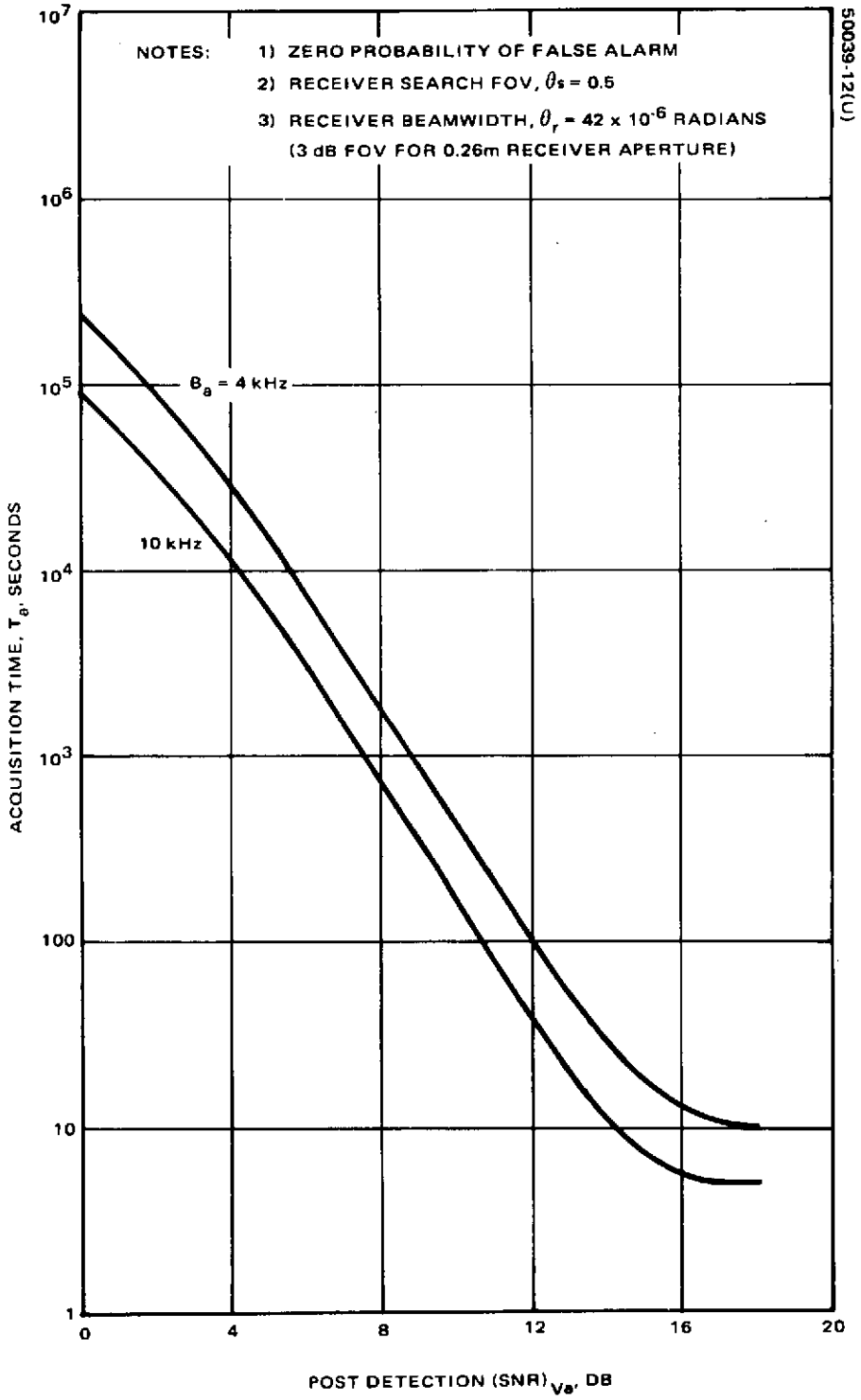

FIGURE 3-2. ACQUISITION TIME VERSUS POSTDETECTION $(SNR)_{Va}$

where B_A is the acquisition bandwidth and Q_1 and P_D the false alarm rate and detection probability associated with the $(SNR)_{Vb}$ at the shuttle beacon receiver. Finally, the total average acquisition time is

$$<T> = T_a + T_A \tag{3-14}$$

Given that the $(SNR)_{Vb}$ at the shuttle beacon receiver will be very large, it is expected that T_A is given by the equivalent to Equation 3-3 for the shuttle beacon receiver

$$T_A = \frac{k}{2B_A}\left(\frac{\theta_{I\ell}}{\theta_t}\right)^2 \tag{3-15}$$

It is seen however from Figure 3-2 that the Molniya may require excessive time T_a to acquire, depending on the $(SNR)_{Va}$ which depends (from Figure 3-1) on the illumination angle $\theta_{I\ell}$ of the shuttle. An acceptable solution is for an $(SNR)_{Va} \geq 14$ dB. This, however, requires an illumination angle of less than 0.2° (for a $B_a = 4$ kHz), which may be interpreted as a requirement of pointing accuracy ±0.1° of the platform which carries the transmitter. The shuttle has a pointing accuracy of ±0.5° and is unsuitable as the platform for the LDRL - 10.6 transmitter. The instrument pointing system (IPS), however, which will be carried by the shuttle, may be utilized for this purpose.

3.2 SHUTTLE TO GROUND LINK

As was mentioned earlier, the dynamics for this link make the link establishment problems more difficult than they are for the shuttle to Molniya link. As a means of reducing this difficulty, the shuttle is elevated to a circular orbit of 500 km.

Figure 3-3 shows the acquisition and track parameters where zenith angle (as viewed from the ground site), tracking angle between the satellite and ground site, and rate of change of this angle are plotted against time. It is assumed that, because of atmospheric effects, the high data rate communications link cannot be established until the zenith angle becomes less than 60°, which occurs approximately 4 minutes after the satellite crosses the ground station's horizon. Acquisition, however, is initiated by the ground station illuminating the shuttle at a zenith angle of 80°, so that 2 additional minutes are available to acquire before the 60° zenith is reached.

The tracking angle at 80° zenith is 65° and the rate is approximately 0.02 deg/sec, whereas at 60° zenith the tracking angle is 52° and the rate is increased to 0.24 deg/sec. The maximum tracking rate occurs at zero zenith angle and is 0.8 deg/sec. Therefore, it is important to achieve

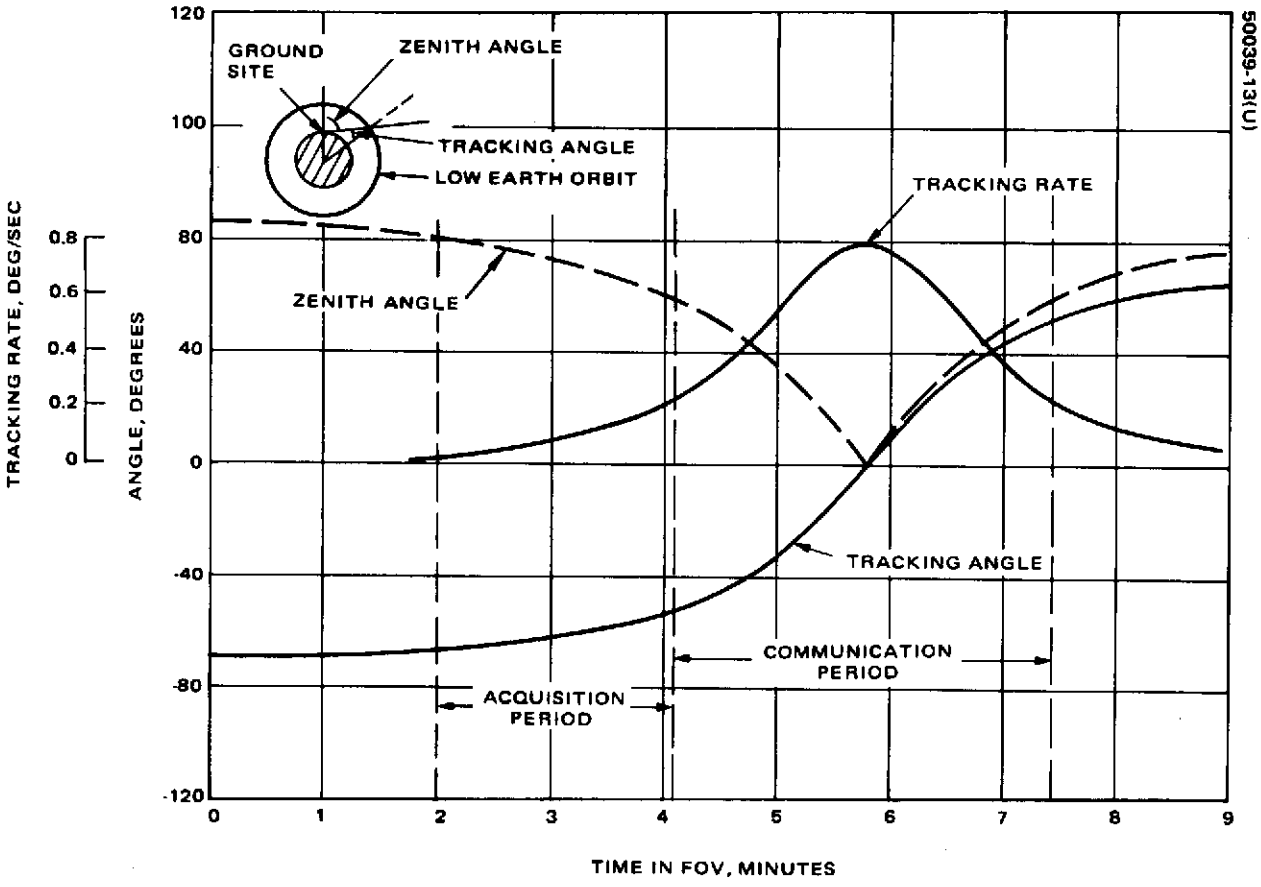

FIGURE 3-3. ACQUISITION PARAMETERS AS FUNCTION OF SATELLITE TIME IN FIELD OF VIEW

acquisition as soon as possible. It is here assumed that acquisition will occur at a zenith angle equal to or greater than 60°, so that acquisition must occur at rates up to 0.24 deg/sec, and tracking must be maintained at rates up to 0.8 deg/sec.

3.2.1 Acquisition Concept

The ground station initiates the acquisition phase by illuminating the shuttle. It is assumed that the power of the ground beacon is great enough that the signal-to-noise ratio in a 6 μsec acquisition pulse is at least 30 dB, so that the probability of detection $P_d \sim 1$ and the false alarm rate is $Q_o \sim 0$. Therefore, the problem of acquisition is one of first bringing the target into the ±0.5° telescope field of view and, second, moving the target across the detector at such a rate that tracking can be initiated.

For the acquisition rates shown in Figure 3-3, there are basically two approaches available for beacon acquisition: 1) use a line scan (fence) and let the relative motion bring the ground beacon across the fence or 2) continuously direct the gimbals to the known position of the ground station so that the relative beacon motion is effectively cancelled.* The concept proposed here is based primarily on the latter approach, but the requirements are formulated such that the former approach can also be used. That is, even though effectively canceling the ground beacon motion through open loop gimbal commands is planned, the specified IMC dynamics will handle target rates up to 0.25 deg/sec using a fence scan.

The proposed concept is described as follows. The inertial gimbal angles and rates are transmitted to the servo system as the following five values:

t_1 = time to execute command

θ_1 = initial value of roll gimbal

$R\theta_1$ = initial rate of roll gimbal

ϕ_1 = initial value of pitch gimbal

$R\phi_1$ = initial rate of pitch gimbal

At execution time t_1, the servo command electronics will generate and execute a command waveform of the appropriate shape (step plus ramp). After executing the first command, five new numbers are transmitted corresponding to the new set of commands to be executed at time t_2 and so on until acquisition takes place.

---

*This assumes that the position of the ground beacon in shuttle coordinates is known to a certain accuracy at all times and can be predicted ahead of time on the basis of ephemeris data.

The command sequence is illustrated in Figure 3-4. As the gimbal angle (pitch angle is illustrated) grows smaller in absolute value (which means the zenith angle is getting smaller) the required time interval between updates also grows smaller because of the higher rates. The frequency of the updates at any point depends on the allowable error between the commanded gimbal position and the desired position. If the allowable error is 10 percent of the 1 field of view, the minimum time interval between updates is approximately 20 seconds for the first minute and reduces to 5 seconds by the end of the third minute.

The foregoing sequence should ensure that the target will remain in the ±0.5° field of view long enough for the IMC to scan the detector across the ground beacon. A spiral scan is proposed which makes use of a single scan frequency and a sawtooth amplitude scan. The optics' effective field of view is further extended through use of a gimbal scan. This proposed gimbal scan, illustrated in Figure 3-5, consists of five discrete positions of the gimbals. The gimbals will be stepped rapidly from one position to the next, but remain at each position long enough for an IMC scan frame to be completed. It is emphasized that the only purpose of the gimbal scan routine is to provide margin between the ±0.5° field of view and the pointing accuracy of the shuttle, which is given as ±0.5° with a rate stability of either 0.01 or 0.1 deg/sec, depending on whether the RCS vernier jets are used (Reference 6); it is assumed that the vernier jets are used.

The acquisition concept can be summarized as follows:

1) From shuttle navigation data the position of the ground beacon is known to a certain accuracy at all times and can be predicted far enough in advance to allow a command sequence to be generated.

2) The command sequence is transmitted to the transmitter servo system and executed at a rate which minimizes gimbal errors so that most of the target error is contributed by the shuttle pointing error.

3) The shuttle pointing error is nominally equal to the telescope FOV (±0.5°), so that the above procedures should bring the ground beacon within the telescope FOV.

4) To add margin to the above procedure, a simple gimbal scan routine is proposed, which extends the effective telescope FOV by a factor of approximately two.

5) Within the telescope FOV, two IMC spiral scans are employed: a large scan covering the entire telescope FOV, which initially brings the ground beacon across the detector, and a mini scan which "zeros in" on the target for capture.

6) A backup is provided in which the spiral scan would be replaced with a circular fence scan and the the gimbal command sequence would be eliminated.

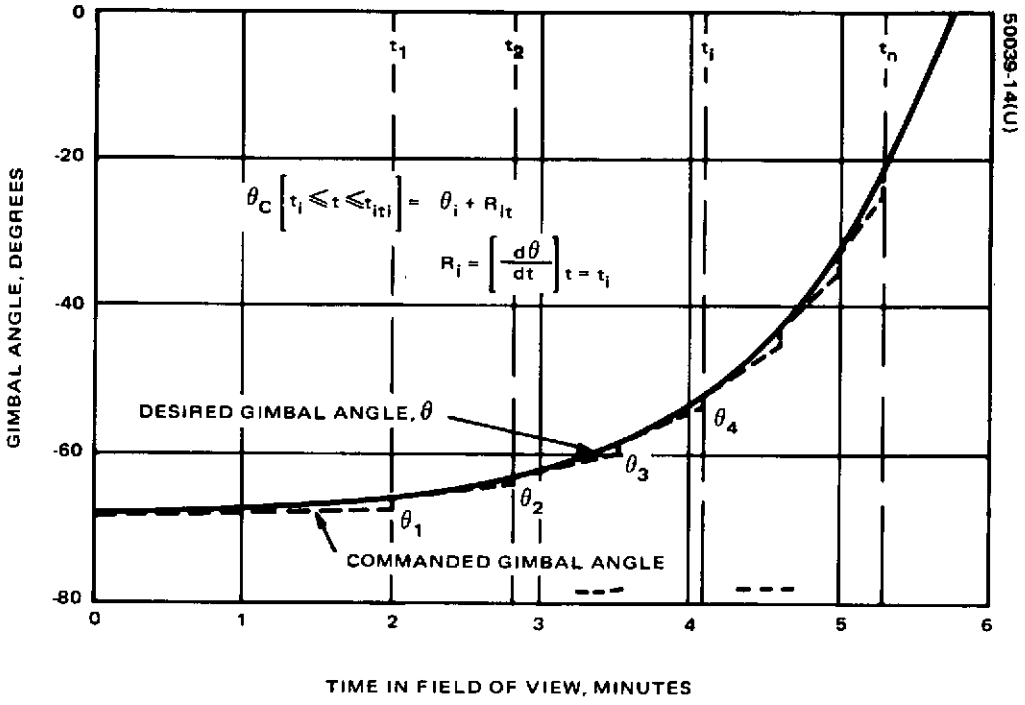

FIGURE 3-4. SKETCH SHOWING GIMBAL COMMAND SEQUENCE

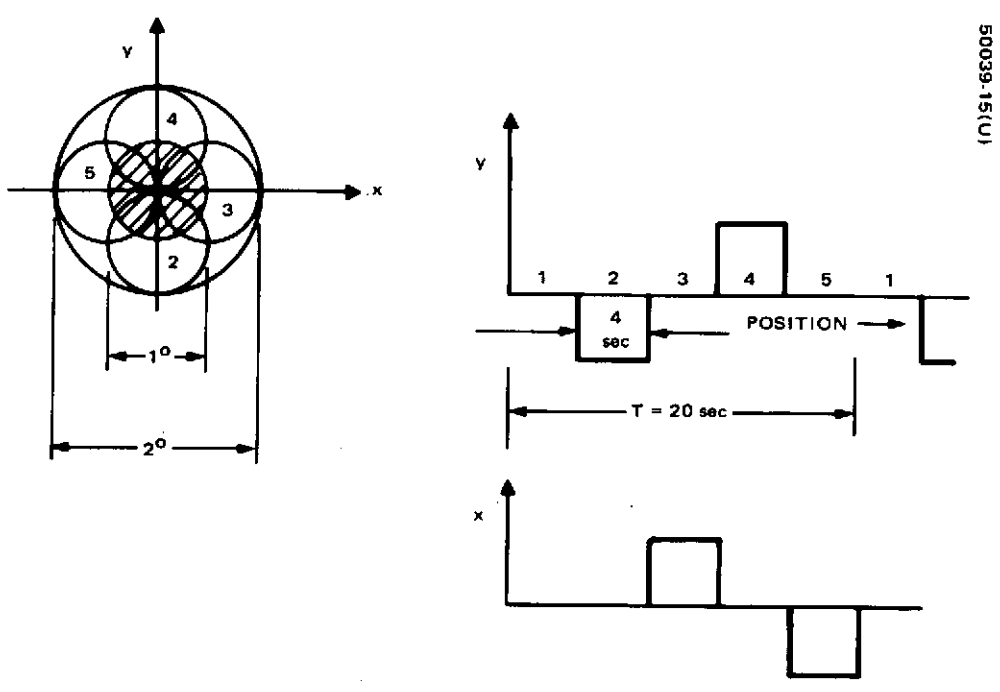

FIGURE 3-5. GIMBAL SCAN ROUTINE

4. LDRL - 10.6 OPTICAL ANALYSIS

4.1 INTRODUCTION

During the design study phase, an effort was undertaken to develop a preliminary optical design for a laser transmitter that satisfied all the design constraints for the LDRL - 10.6 space shuttle experiment. In addition to meeting the design specifications, the prime effort was directed toward maximizing the energy transfer through the optical system. Previous trade-off studies (see Reference 5) of system configurations have established that an afocal Gregorian telescope provides the best design solution for a laser transmitter. This design type minimizes the central obscuration of the transmitted beam, and the confocal arrangement of the folded Gregorian system leads to zero spherical aberration on-axis and negligible coma and astigmatism off-axis. The Gregorian design also permits the entrance pupil to be located externally without the need for an auxiliary relay system.

Although this study was principally oriented toward the system design for a transmitter, it is recognized that the transmitter and beacon receiver will share common optics (at least in the beam expander portion) in order to reduce the overall size and weight requirements.

Preliminary tradeoffs requiring evaluation for the design of an efficient laser transmitter/receiver include the following:

- Field of view, f number of the primary and secondary mirrors, primary mirror diameter, magnification ratio, and the effects due to a central obscuration
- Beam matching techniques
- Off-axis power losses due to vignetting

These tradeoffs will be examined in detail in subsection 4.4. First, however, a brief introduction into the rationale that goes into the preliminary design effort for a space-borne laser communication system follows. This introduction will include several techniques for implementing the specified optical design parameters and some of the problems associated with their use.

4.2 OPTICAL DESIGN CONSIDERATIONS

The size and shape of the primary aperture determines the maximum antenna gain or on-axis peak intensity achievable for a given optical communication system. Because of this, large aperture optics are theoretically attractive for their high antenna gain values. As one doubles the radius of the primary, the antenna gain (energy in the far field) increases by a factor of 4. However, practical considerations persuade one to utilize only as large an aperture as is necessary. In addition, smaller aperture optical communication systems lend themselves to simpler and more reliable point and track instrumentation as well as being less sensitive to vibration and distortions due to temperature gradients. Most importantly, the size of the aperture of the optical system must be compatible with achieving a system whose weight and cost are minimized.

The design consideration determining how much energy is transferred through the optical train is the obscuration ratio; it is defined to be the fraction of area of the entrance pupil that is blocked by the image of the central hole in the small folding mirror (see 4.5). This obscuration has a great effect on the transmitted energy output because the Gaussian beam profile of a CO_2 laser has its highest energy concentration in the center of the beam. Figure 4-1 shows a comparison of the percent energy obscured for uniform and Gaussian beam for a 7-inch aperture, the Gaussian beam being truncated at the $1/e^2$ point. The central obscuration of the Gregorian telescope is essentially determined by the inside aperture of the small folding mirror. The size of this aperture is in turn determined by the telescope acquisition field of view, ±0.5°; this situation occurs because the inside aperture must be sufficiently large so that no part of the image field of the incoming beacon beam is obscured during acquisition. The size of the image field, η, at the focal plane of the primary mirror is given by

$$\eta = f \cdot \theta$$

where f is the focal length of the primary mirror. For the LDRL - 10.6 laser transmitter, θ = 17.45 mrads (i.e., 1°). Thus, for a given θ and primary mirror diameter, D, the central obscuration can be minimized only if f is minimized. This implies that the f number (= f/D) of the primary must be small if the power loss resulting from central obscuration is to be minimized.

The actual obscuration is slightly larger than the calculated value to allow for manufacturing tolerances in centering and aligning the optical system. For the LDRL-10.6 design, 1 mm of decentration tolerance was allowed in calculating the obscuration ratios.

Based upon practical experience, the f number of the primary should not fall much below f/1.5, or the misalignment tolerances will become extremely small. Here the advantage of having a fast primary could easily be canceled by the performance degradation resulting from residual misalignments (Reference 4).

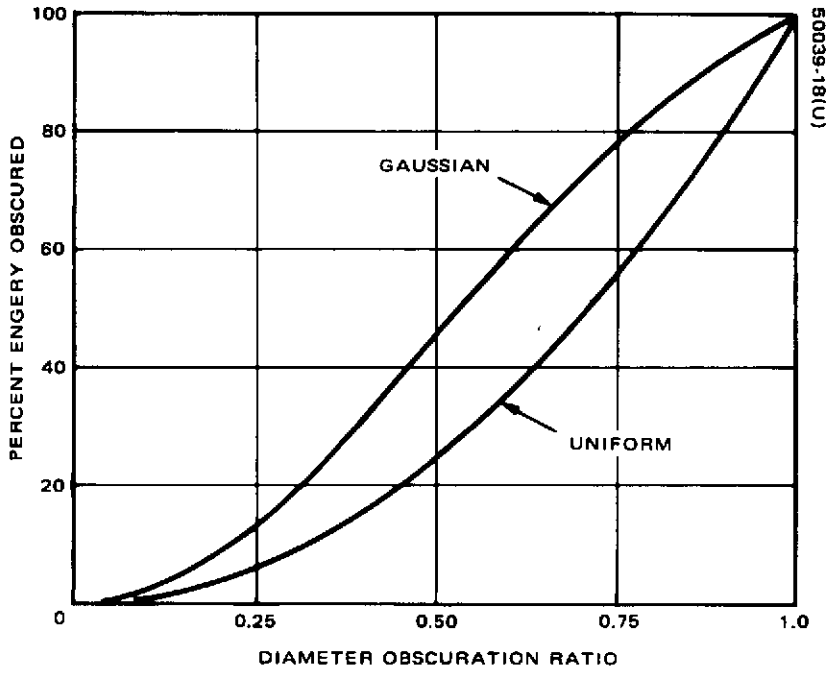

FIGURE 4-1. TOTAL ENERGY OBSCURED FOR UNIFORM AND GAUSSIAN BEAMS USING 7 INCH APERTURE

Another consideration is the design configuration of the beam expander optics. This configuration can be either refractive, reflective, or catadioptric, in any of the possible combinations or modifications of classical telescope designs (i.e., Cassegrainian, Schmidt, Galilean, etc). The function of the telescope beam expander is to expand the signal beam from a laser source to a size compatible with an aperture based on the antenna gain requirements of the system. Beam expanders usually consist of all-reflective elements due to the possibility of widely different wavelengths used for the transmitter and receiver channels. Also there are greater light-weighting possibilities with all-reflective designs. The design requirements of the beam expander will be further discussed in 4.3.

4.3 OPTICAL FEATURES

The following are general design features which were considered in the preliminary design of the LDRL-10.6 space communication system:

1) The transmitter must be designed to be diffraction limited and is always pointed at the receiver with an angular pointing error which is small in comparison to the diffraction beam spread.

2) The alignment error between the transmitter and receiver must be small compared to the diffraction angle of the transmitter antenna. This requirement usually leads to the practice of having the transmitter and receiver share the same antenna.

3) A deliberate offset or point-ahead angle must be added to the boresight adjustment between the transmitter and receiver.

The following paragraphs are a discussion of these and other features which must be incorporated into the design for a successful laser communication system.

4.3.1 Beam Expander Optics

The beam expander is an afocal telescope that transforms a small diameter, collimated laser beam into a beam of larger diameter with less divergence. Beam expander optics are considered to be common to both the transmitter and the beacon receiver. The size of the beam expander output aperture determines the maximum achievable antenna gain for both the beacon receiver and transmitter. The field of view of the beam expander will be determined primarily by the IMC and acquisition requirements. These FOV requirements in combination with thermal and mechanical constraints determine the f number of the components of the beam expander. Another restriction on the beam expander design is that it provides a pupil location which is accessible to the IMC function.

4.3.2 Image Motion Compensation

Success of a laser communication system necessitates that the aimpoint of the narrow beamwidths of these systems be maintained with great stability. The output pointing direction must be isolated from the angular motions of the shuttle platform to a small fraction of the transmitter beamwidth. In order to achieve the necessary mirror response bandwidths with a minimum of power, it is desired that the optical element of the IMC that performs this task have as low an inertia as possible. The preferred location for this function is at, or very close to, the stop position as shown in Figure 4-11, where the diameter of the optical aperture is smallest. The pointing angle range of the IMC device must be wide enough to accommodate the largest residual angular motions permitted by the gimbal pointing or shuttle stabilization requirements. Initial acquisition between the shuttle and receiver station can also utilize the IMC components to provide a search/scan function.

4.3.3 Initiation of Acquisition Sequence

The acquisition sequence of the transmitter receiver linkup can be initiated by injecting a suitably small diameter laser beam into the transmitter optics. The corresponding output beam serves as a transmitter beacon, and the initial acquisition sequence then consists of the receiver searching for this beacon beam. Now, if the axis of this beam is accurately aligned parallel to the output axis of the transmitter, and if the angular diffraction spread of this beam is matched to the desired field of view for the initial acquisition, a beacon lock-on by the receiver establishes the relative angular position between the receiver and the transmitter to within the acquisition tolerance.

4.3.4 Point Ahead Optics

Due to the relative orbital velocity of the shuttle and the receiver station and the finite velocity of light, the pointing direction of the receiver beacon does not automatically provide the exact indication of the location of the receiver. Therefore, it is not appropriate to direct the transmitter's output beam in the apparent direction of the beacon but rather aim it toward the receiving station location at the time the light travels that distance. Thus, a "point-ahead" correction must be introduced between the pointing direction of the receiver and transmitter. For the LDRL-10.6 system, it is proposed that the point-ahead correction be incorporated into the beacon-receiving channel. A pair of Risley prisms (see Figure 4-2) are convenient means of accomplishing the point-ahead function. The offset is obtained by rotation of one prism to obtain the desired magnitude and rotating both prisms together to obtain the desired direction. The information for point-ahead changes slowly with time and can be telemetered to the Risley prism servo from the ground station. In addition, the point-ahead optics can be used to compensate for any boresight shift between the transmit and receive channels.

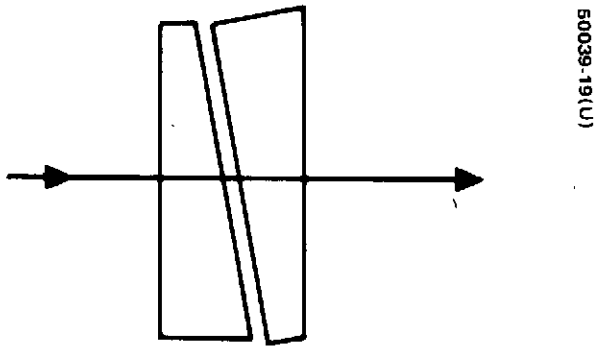

50039-19(U)

a) MINIMUM DEVIATION

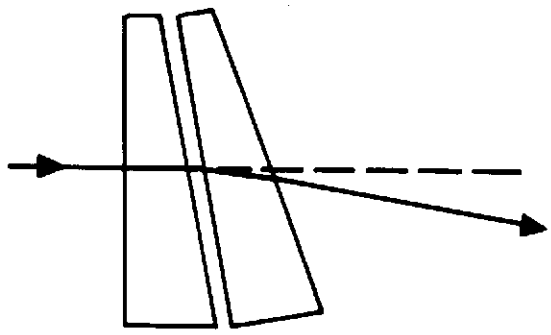

b) MAXIMUM DEVIATION

FIGURE 4-2. RISLEY PRISM ASSEMBLY

4.3.5 Energy Redistribution Devices

The Gaussian profile TEMoo basic laser mode has its highest energy concentration in the center of the beam. This central portion of the beam is lost in a normal obscured aperture beam expander. Several methods have been devised for reconstituting the intensity profile of laser beams to reduce this loss due to central obscurations. One such device that was examined is the axicon. The energy redistribution axicon shown in Figure 4-3 can increase far field peak intensity by a factor of 2 when the central obscuration is 25 percent (Reference 7). Figure 4-4 compares antenna gains as a function of obscuration ratio for an optical telescope illuminated with a uniform irradiance beam, a Gaussian beam, and a Gaussian distribution as modified by an axicon. Alignment tolerances for this technique tend to be quite critical. The increased gain anticipated from the use of an axicon must be weighed against the possible degradation due to residual manufacturing errors. An additional consideration is the axicon's high cost of manufacturing to the required tolerances. Subsection 4.6 is a further evaluation of the axicon device. Some anticipated technical difficulties, together with the uncertain hardware delivery schedule, have precluded the use of axicon in the present design of the transmitter system.

Another method of reconstituting the Gaussian beam profile so as to minimize the output losses resulting from the central obscuration is to suitably expand the beam to overfill the aperture stop of the telescope. By broadening the beam profile, the high energy central region will be spread more, and consequently a given obscuration ratio will cut off a smaller portion of the laser energy. The increase in the output power is achieved by truncating the lower power $1/e^2$ regions of the beam profile and passing more of the high power regions. This was the technique that was considered in the LDRL-10.6 preliminary design, and will be examined more fully in 4.4.

4.4 TRADEOFF ANALYSIS OF GREGORIAN AFOCAL BEAM EXPANDER

A number of Gregorian afocal systems have been examined with the aim of selecting a best-compromise optical design solution for the LDRL 10.6 space shuttle experiment. In this tradeoff study, two output beam diameters, 8.8 and 7 inches, have been considered. For the 8.8-inch output beam, the following tradeoff parameters have been examined:

Diameter of primary mirror

f number of primary

Afocal magnification (and input beam size)

Obscuration ratio

Input-beam matching (to the Gregorian beam expander)

Power output versus field position

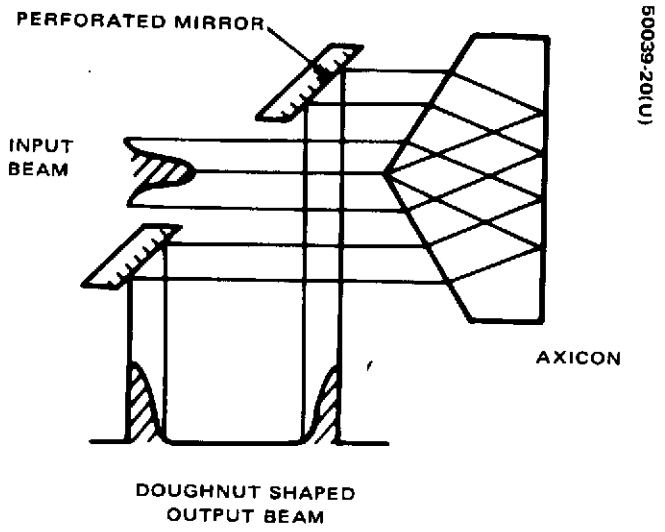

FIGURE 4-3. ENERGY REDISTRIBUTION TECHNIQUE

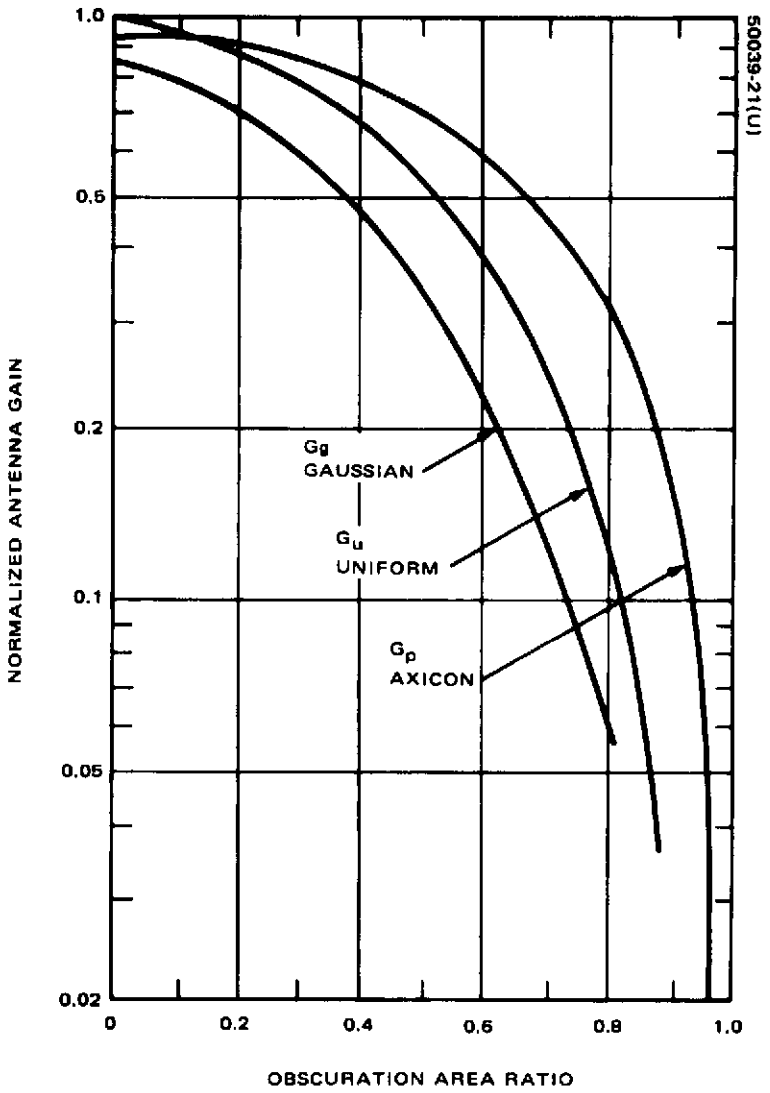

FIGURE 4-4. NORMALIZED ANTENNA GAIN FOR OPTICAL TELESCOPE ILLUMINATED WITH UNIFORM INTENSITY WAVEFRONT (G_U), TEM_{00} LASER MODE OUTPUT (G_g), AND GAUSSIAN DISTRIBUTION REDISTRIBUTED WITH AXICON (Gp)

Based on the results of this tradeoff study and fabrication cost estimate, it was concluded that a smaller 7-inch output beam would provide a good compromise between the overall performance and cost. The selected design comprises an f/1.5 primary mirror of 7 inches diameter, and the Gregorian afocal beam expander has a magnification ratio of 7X and an area obscuration ratio of approximately 0.17.

This subsection presents the results associated with tradeoff parameters for both the 8.8 and 7-inch output beams. Details related to the selected optical design, together with a preliminary layout, are discussed in 4.5.

4.4.1 Gregorian Afocal Beam Expander for 8.8-Inch Output Beam

It has been pointed out in 4.2 that the central obscuration of the Gregorian system is dependent on the product of the focal length of the primary and the acquisition field angle in radians. Since the acquisition field angle is fixed (±1/2° or ±8.726 mr), it would therefore be useful to study the effects of different primary focal lengths upon the central obscuration of the system. For this study, it is more meaningful to consider the f number (= focal length of primary/diameter of primary) rather than the focal length, and the diameter of the primary mirror is set equal to the 8.8-inch output beam diameter. Two magnification ratios, M = 10X and M = 9X, were first considered. The reason for choosing these Ms was based on the fact that the IMC size was limited to accommodating input beams no larger than 1 inch in diameter. Figure 4-5 shows the graphs of area obscuration ratio versus f number of primary mirror, for M = 10X and 9X. It is clear from these graphs that the area obscuration increases rapidly with primary f number, and that M = 9X is more preferable than M = 10X. Based upon practical experience, the f number of the primary should not fall much below f/1.5, or the misalignment tolerances would become extremely small. In the subsequent tradeoff studies, f/1.5 aperture was taken to be the nominal f number for the primary mirror.

Figure 4-6 presents the plots of area obscuration ratio versus the afocal magnification, M, for Gregorian beam expander with f/1.5 and f/2.0 primaries. Since the output beam diameter was taken to be a constant 8.8 inches, different M implied different input beam sizes. As pointed out earlier, the dimensions of the IMC required M to be greater than 8.8. The graph shows that a good compromise is achieved with an f/1.5 primary in combination with a beam expander ratio of M = 9; larger values of M and f number of primary will result in unacceptable power transmission losses.

The question of input beam matching to the Gregorian beam expander has been examined for systems with f/1.5 primary and M = 9 and 10. The approach was based on the fact that the Gaussian beam from the CO_2 laser could be suitably expanded so as to overfill the entrance pupil of the beam expander. By broadening the beam profile, the high energy central region would spread out more, and consequently, a given central obscuration would

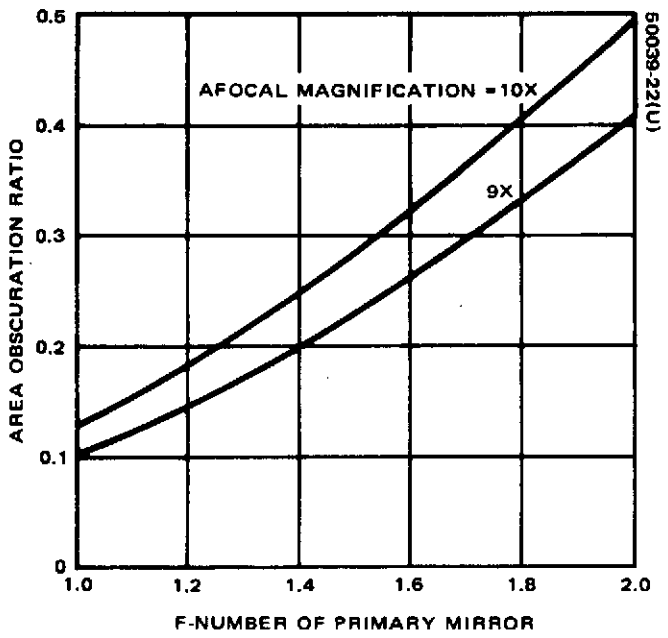

FIGURE 4-5. AREA OBSCURATION RATIO VERSUS F NUMBER OF PRIMARY MIRROR FOR AFOCAL MAGNIFICATIONS OF 10X AND 9X (OUTPUT BEAM DIAMETER, 8.8 INCHES)

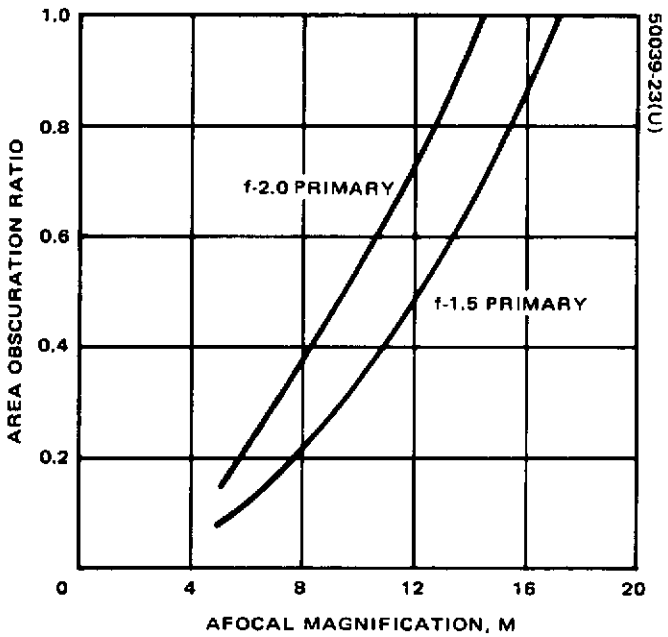

FIGURE 4-6. AREA OBSCURATION RATIO VERSUS AFOCAL MAGNIFICATION, M, FOR F/1.5 AND F/2.0 PRIMARIES (OUTPUT BEAM DIAMETER, 8.8 INCHES)

cut off a smaller portion of the laser energy. The increase in the output power could, therefore, be achieved by truncating the low power $1/e^2$ regions of the beam profile and passing more of the high power regions.

Figure 4-7 presents the transmitted power ratio versus the beam matching parameter for the Gregorian beam expanders with f/1.5 primary of 8.8 inch diameter, and M = 9 and 10. The transmitted power ratio is defined as the ratio of the power transmitted through the beam expander in the presence of central obscuration, to the power of the input Gaussian laser beam. The laser beam is truncated at the $1/e^2$ point with a corresponding beam width of W. The beam matching parameter is defined as the ratio D/W, where D is the diameter of the entrance pupil of the beam expander. The ratio D/W is, therefore, less than unity if the laser beam width is overfilling the entrance pupil. Figure 4-7 shows that the transmitted power is maximized if D/W is 0.98 for M = 9 and 0.93 for M = 10.

For the particular case corresponding to the beam expander with f/1.5 primary of 8.8 inch diameter and with D/W = 0.98 and M = 9, the transmitted power ratio versus field angle is plotted in Figure 4-8. Referring to this figure, the transmitted power ratio is the transmitted power through the beam expander at a given output field angle, normalized by the power of the laser source. The lower curve in Figure 4-8 shows that the off-axis transmitted power is only slightly degraded, even though there are considerable amount of vignetting (resulting from off-axis beam translation). The reason for this slow fall-off is because as the input beam is steered off-axis by the IMC, the central portion of the Gaussian beam is no longer completely obscured by the cutout in the small folding mirror (see 4.5); the energy lost by vignetting the low-power $1/e^2$ region of the Gaussian beam is partially made up by passing more of the high-power central region.

The upper curve in Figure 4-8 shows the effect of increasing the diameter of the primary mirror from 8.8 to 10 inches, but keeping its focal length and other design specifications unchanged. The larger primary mirror leads to reduced vignetting for the off-axis beam; this effect, together with the increased passage of central region of the Gaussian beam for off-axis output (see above) result in a net gain in the transmitted power as the field is increased from 0° to ±1/2°. The area obscuration ratio for both the 8.8 and 10-inch primary systems was 0.23.

4.4.2 Gregorian Afocal Beam Expander for 7-Inch Output Beam

A follow-on study has also been carried out for a Gregorian afocal beam expander using a 7-inch diameter f/1.5 primary mirror and M = 7X. This system was considered as a result of studying the f/1.5 curve in Figure 4-6: this particular curve showed that the area obscuration fell rapidly as M was reduced; to take advantage of this effect, a new, smaller magnification ratio M = 7 was selected. The input beam size was taken to be 1 inch and the overall size of the primary mirror was 7 inches. Although the latter mirror dimension would vignette part of the off-axis output beam, the actual

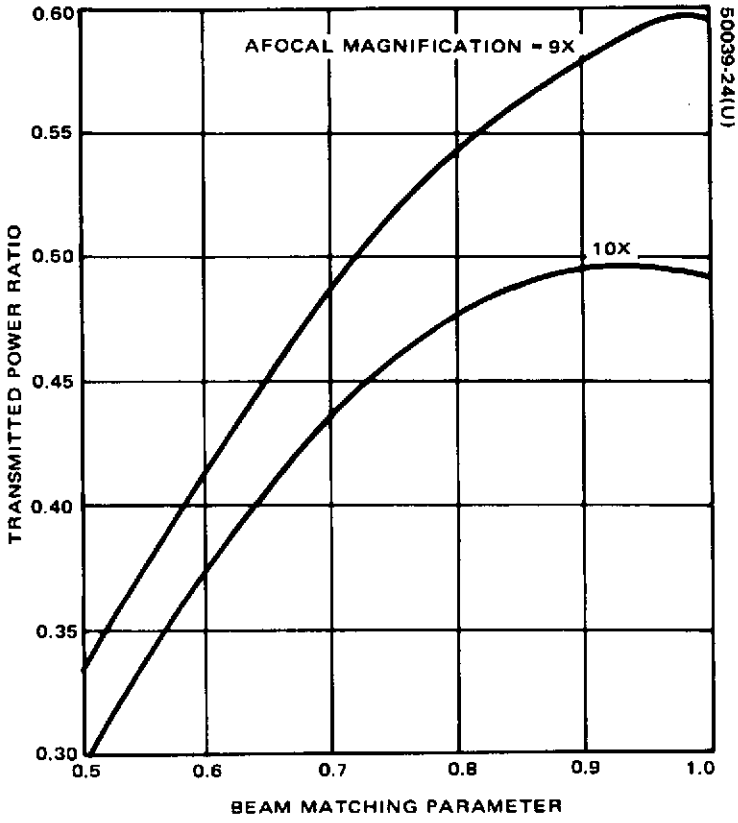

FIGURE 4-7. TRANSMITTED POWER RATIO VERSUS BEAM MATCHING PARAMETER (OUTPUT BEAM DIAMETER, 8.8 INCHES; PRIMARY MIRROR, F/1.5)

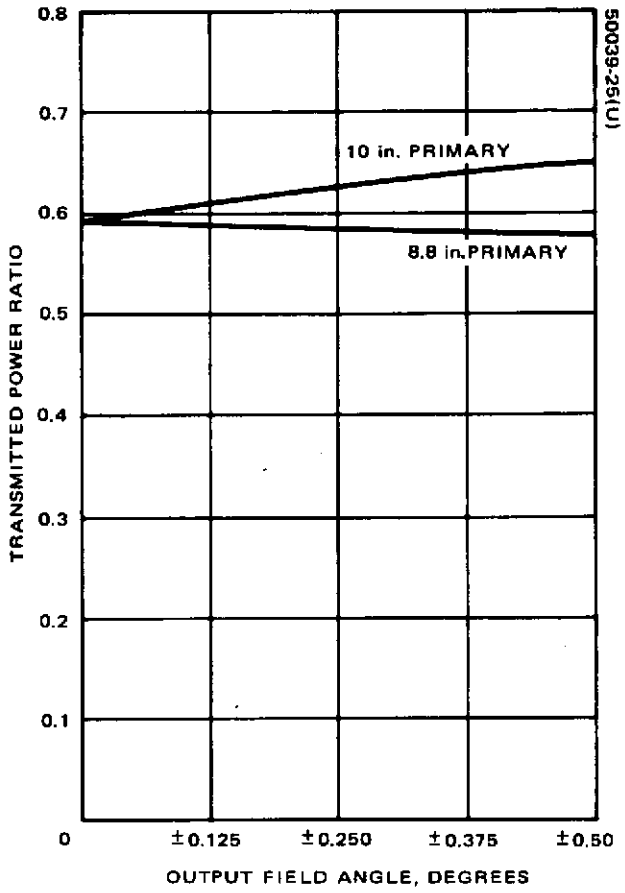

FIGURE 4-8. TRANSMITTED POWER RATIO VERSUS OUTPUT FIELD ANGLE (AFOCAL MAGNIFICATION, 9X; AREA OBSCURATION, 0.23)

loss in the off-axis transmitted power would be almost negligible because of the Gaussian beam profile (see Figure 4-10 and the explanation given above).

The area obscuration ratio for this new beam expander with 7-inch primary mirror was found to be 0.17, which is considerably less than the area obscuration of 0.23 associated with the M = 9 system discussed earlier. It should be pointed out that, although the 7-inch primary system with M = 7 has smaller area obscuration and therefore greater energy transmission as compared with the 8.8-inch primary system with M = 9, the latter system does have higher antenna gain because of the larger aperture size. However, the 7-inch primary system is less costly and, for this reason, it was ultimately selected as the recommended design for the LDRL 10.6 space shuttle experiment. It is useful to mention here that the use of M = 7 instead of 9 has the additional advantage of reducing the overall size of the transmitter package and of minimizing the angular range requirement of the IMC mirrors.

The requirement for input beam matching and the power transmission versus output field have been studied for the 7X Gregorian afocal beam expander. Figure 4-9 presents the plot of the transmitted power ratio versus the beam matching parameter. This figure differs from Figure 4-7 in that the 7X system has a smaller central obscuration. For this system, it is of interest to note that the maximum power transmission is achieved when the beam matching parameter is unity, implying that the input beam width of the CO_2 laser should be 1 inch, equaling the diameter of the entrance pupil of the 7X beam expander. For this optimum input beam matching, the corresponding transmitted power ratio versus the output field is plotted in Figure 4-10. The on-axis transmitted power ratio is given as 0.668, indicating that the central area obscuration of 0.17 has resulted in a power loss of 33.2 percent relative to the power of the CO_2 laser source (see Figure 4-10). The corresponding power loss at the maximum field of $\pm 1/2^\circ$ is 36.2 percent. The reason for this slow fall-off in transmitted power with output field is the same as that given for the lower curve in Figure 4-8.

It should be pointed out that the true limiting aperture of this 7X Gregorian beam expander (see 4.5) is defined by the 7-inch diameter of the primary mirror. Off-axis vignetting of the output beam occurs only at this mirror; all the other optical components in the system are suitably sized so as to avoid further vignetting.

As stated earlier, this 7X Gregorian beam expander has been selected as the recommended design configuration for the LDRL-10.6 space shuttle experiment. Preliminary data for this system are presented in the next subsection.

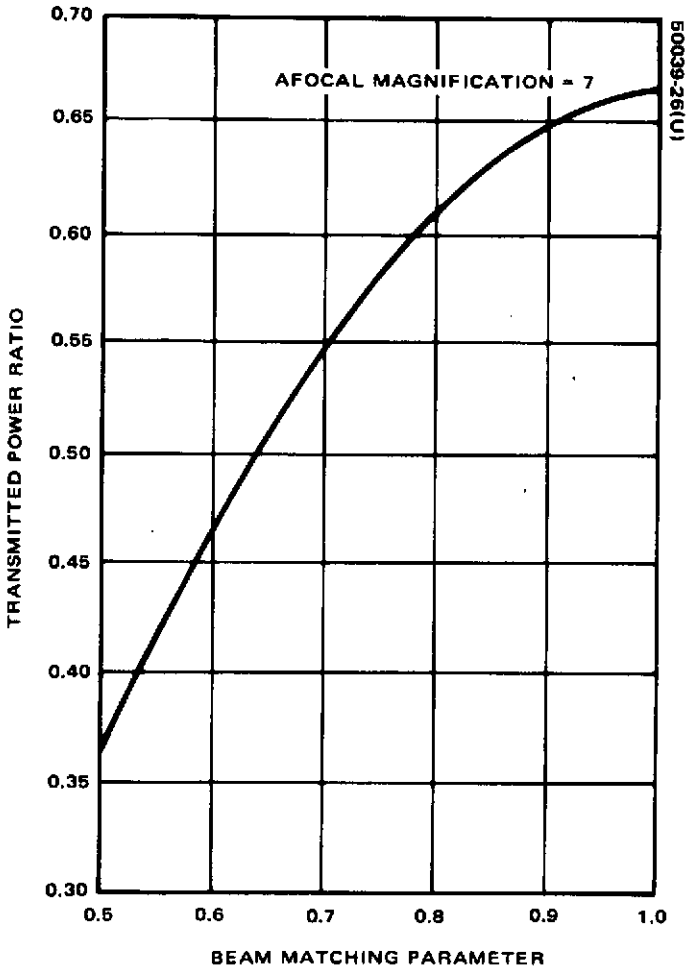

FIGURE 4-9. TRANSMITTED POWER RATIO VERSUS BEAM MATCHING PARAMETER (OUTPUT BEAM DIAMETER, 7 INCHES; PRIMARY MIRROR, F/1.5

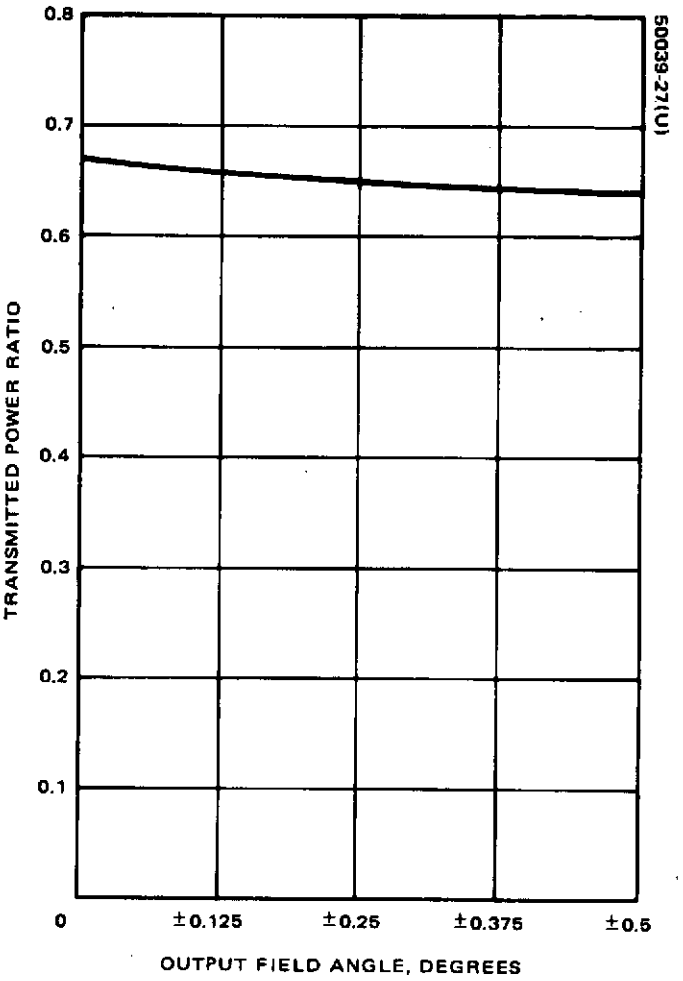

FIGURE 4-10. TRANSMITTED POWER RATIO VERSUS OUTPUT FIELD ANGLE (AXIAL OUTPUT BEAM DIAMETER, 7 INCHES; AFOCAL MAGNIFICATION, 7X; AREA OBSCURATION, 0.17)

4.5 PRELIMINARY DESIGN OF 7X GREGORIAN LASER TRANSMITTER AND BEACON RECEIVER FOR LDRL-10.6 SPACE SHUTTLE EXPERIMENT

A preliminary schematic optical layout and the optical characteristics of the 7X Gregorian afocal system are presented in Figure 4-11 and Table 4-1,

SURFACE	LIMIT RAY HEIGHT*, in.
IMC 1	0.3212
STOP	0.3050
IMC 2	0.59.76
SMALL FOLDING MIRROR	0.7819
SECONDARY MIRROR	0.6071
PRIMARY MIRROR	3.500
LARGE FOLDING MIRROR	5.007
POINTING MIRROR	5.285

*NOTE: DISTANCE MEASURED ALONG THE MIRROR SURFACE

50039-28(U)

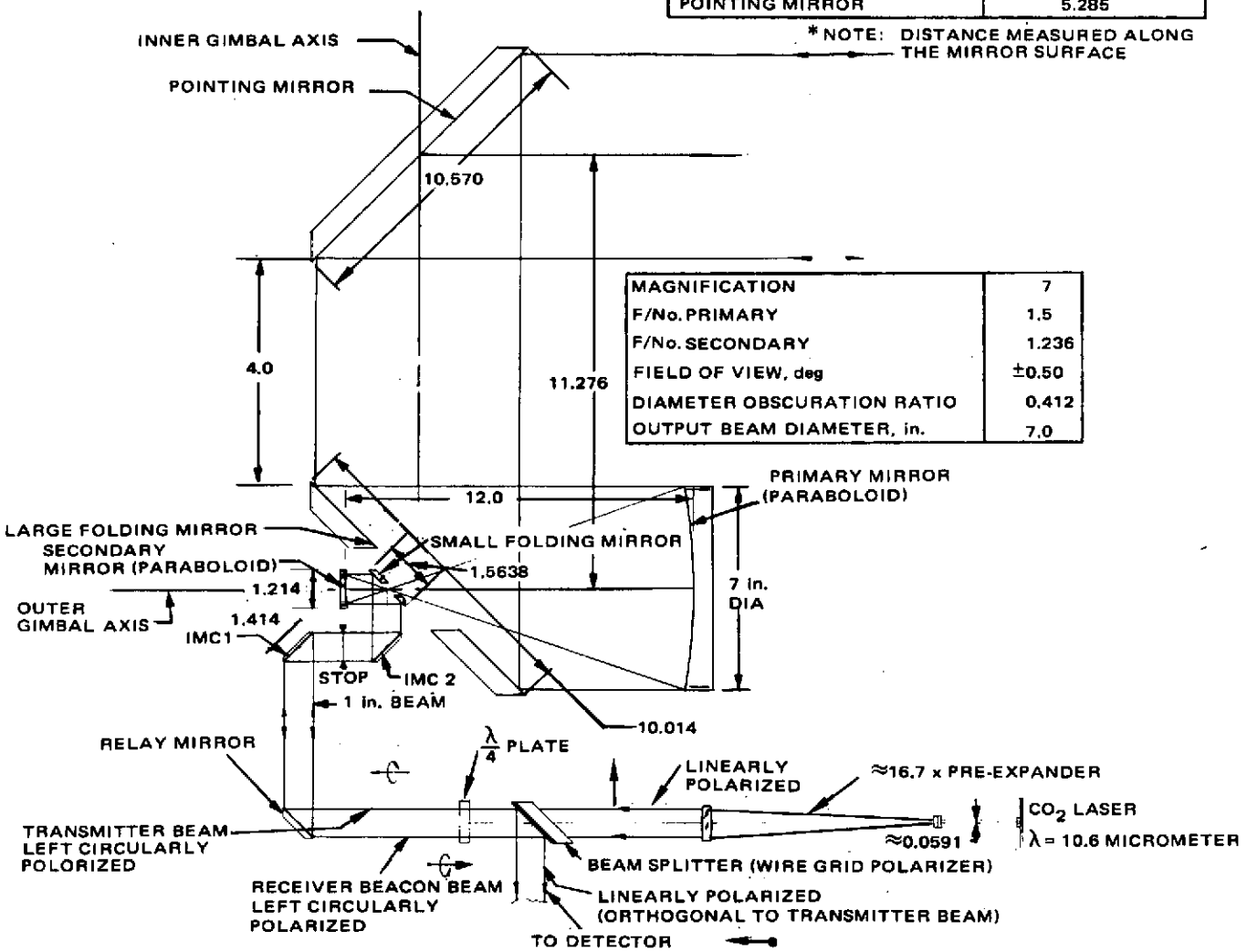

MAGNIFICATION	7
F/No. PRIMARY	1.5
F/No. SECONDARY	1.236
FIELD OF VIEW, deg	±0.50
DIAMETER OBSCURATION RATIO	0.412
OUTPUT BEAM DIAMETER, in.	7.0

FIGURE 4-11. PRELIMINARY OPTICAL LAYOUT OF LDRL, 10.6 7X GREGORIAN BEAM EXPANDER (ALL DIMENSIONS ARE IN INCHES)

TABLE 4-1. OPTICAL CHARACTERISTICS OF 7X GREGORIAN BEAM EXPANDER (PRELIMINARY DATA)

Parameter	Value
Design configuration	Modified afocal Gregorian system with paraboloidal primary and secondary
Diameter of primary	7 in.
Diameter of secondary	1.2 in.
Diameter of on-axis output beam	7 in.
Diameter of stop	1 in.
F number of primary	1.5
F number of secondary	1.236
Afocal magnification	7X
Output field of view	$\pm 0.5^{o}$
Separation: primary/secondary	12 in.
Spectral region	10.6 μm
Area obscuration ratio	0.17
IMC dimension	1 x 1.414 in.

respectively. The linearly polarized, modulated output beam from the CO_2 laser device has a diameter of approximately 0.06 inch (see Figure 4-11). This beam is pre-expanded to 1-inch diameter, and then transmitted through the beam splitter and the $\lambda/4$ plate. The beamsplitter is actually a wire-grid polarizer; this polarizer, together with the $\lambda/4$ plate, converts the transmitted beam into a right-handed, circularly polarized beam. This beam is then directed by relay mirrors (only one is shown in Figure 4-11) toward the IMC mirrors 1 and 2. The reflected beam then enters the Gregorian afocal beam expander via a small folding mirror with a central cutout. The beam expander consists of confocal paraboloids with the common focus located at the center of the small folding mirror. The f numbers of the paraboloidal primary and secondary mirrors are 1.5 and 1.236, respectively. Situated in between the small folding mirror and the primary is a large 45° folding mirror; the central cutout of this mirror is matched to that of the small folding mirror so as to permit the reflected beam from the secondary to reach the primary mirror. The expanded beam reflecting off the primary is collimated, and has a beam diameter of 7 inches. This beam is then reflected off the large folding mirror toward the pointing mirror along the inner gimbal axis. The final output beam is directed by the pointing mirror to the distant receiver target. The 2-axis pointing capability is achieved by rotating the pointing mirror about the inner gimbal axis and the beam expander about the outer gimbal axis. The latter also coincides with the optical axis of the beam expander.

The stop of the system and the entrance pupil are both located at the midplane between the two IMC mirrors. The diameter of the stop is 1 inch.

The central area obscuration ratio of the system is 0.17, corresponding to a diameter obscuration ratio of 0.412. The large beam obscuration occurs at the center of the small folding mirror; the size of this obscuration is determined by the telescope acquisition field of view of ±0.5°. Details related to this have been considered in 4.2. The transmitted power ratio versus the output field (up to ±0.5°) is plotted in Figure 4-10, and the results are discussed in 4.4. The preliminary limiting ray heights at the key elements of the optical train are presented in Figure 4-11; the corresponding output field angle considered is +0.5°.

When the Gregorian telescope is used in the receiving mode for initial acquisition, the incoming beacon beam within the acquisition field of ±0.5° is directed by the pointing mirror into the telescope via the large folding mirror. The beacon beam emerging from the IMCs is now demagnified by 7X. The state of polarization of this beacon is left-handed, circularly polarized, which is the reverse of the outgoing transmitter beam. This beacon beam, after passing through the λ/4 plate, will now be reflected off the wire-grid polarizer (beamsplitter); the state of polarization of this reflected beacon beam is linear, but orthogonal to the plane of polarization of the transmitter beam coming out of the CO_2 laser device.

As discussed in 4.2, the point ahead device is to be positioned in the beacon/receiving channel. The location of this device should therefore be in between the beamsplitter and the PMT detector package for the beacon.

4.6 FURTHER EVALUATION OF THE AXICON DEVICE

It has been pointed out in 4.3 that, because of anticipated technical difficulties together with the uncertain hardware delivery schedule, the use of the axicon device was precluded from the present design of the transmitter system. Nevertheless, it is useful to present here an account of the factors considered in the tradeoff evaluation of the device. Technical discussions have been carried out with two vendors (Perkin-Elmer Corp. and Applied Optics Corp.).

The following five topics were considered in the tradeoff:

1) Polarization effects

2) Light scattering

3) Cost

4) Testing

5) Material

4.6.1 Polarization Effects

The refracting axicon offering the best tradeoff is an inverted axicon, which has an aluminized back surface. The small critical angle for Ge requires that the back surface adds a small difference in reflectance for the S- and P-states of polarization. There is also a 180° phase difference between the S-P states at the aluminized surface. For the all-reflecting axicon, the polarization at the aluminized front surfaces experience both polarization and phase changes for the S- and P-states.

4.6.2 Light Scattering

Normally, axicons are placed on a spindle and rotated with a polishing pad placed against the surface. The center "point" in this configuration does not rotate, and thus the top 1/2 mm is several wavelengths off from a true cone, due to the lack of polishing at the tips of the axicon. Perkin-Elmer can provide a lap moving along the surface and thus can polish to the tip of the axicon, with the effect of reducing back scattering.

4.6.3 Cost

The above mentioned Perkin-Elmer lap method of polishing takes approximately 200 hours of optical polishing at $24.00 per hour for a total of $4800.00 with an approximate material cost of ZnSe of $600.00 (from Raytheon). First estimate of the cost of a "good" conical-shaped ZnSe axicon (1/2 inch thick and 2 inch diameter) is $10,000.00.

4.6.4 Testing

The choice of ZnSe over Ge is attributed to the reasonable cost of testing. Essentially ZnSe can be tested with red light because its transmission extends to the visible portion of the spectrum so that one can "see" through it. It also has a lower absorption at 10.6 μ. ZnSe can be tested by examining the fringe pattern for scanning rings to determine the flatness of the axicon tip. To test Ge, an IR source must be used with a detector. The signal is subsequently digitized and read out on oscilloscope. The testing is difficult and expensive for Ge.

4.6.5 Material

The selection of nontoxic, IR, low absorption material is limited to Ge and ZnSe. The ease in testing the latter appears to make it the better choice.

5. STRUCTURE AND BEAM STEERING CONTROL MECHANISMS

The structure consists of three basic beryllium subassemblies as follows.

The base is a compartment, containing provisions for being hard-mounted to a spaceframe and provides space for the installation of detector, communication, and other electronic equipment. Items required for servo instrumentation (resolver, encoder, and tachometer for the outer gimbal drive) are included in the base.

The outer gimbal is a rotatable compartment driven from the base containing a large 45° folding mirror, the primary and secondary focusing mirrors, the image motion compensators and field stop, and such folding mirrors as required to direct the beam through the IMC path and back to the base compartment centerline. The servo instrumentation items for the inner gimbal are mounted on the outer gimbal subassembly. Two angular contact bearings support this gimbal to the base.

The inner gimbal is a rotatable element containing a 45° pointing mirror for directing the beam to the remote receiver. Two angular contact bearings support this inner gimbal to the outer gimbal.

Beam steering control includes the gimbals with the associated drives to achieve the 2π sr coverage and ensure beam control, and the image motion compensators for fine beam control.

5.1 GIMBAL DRIVES

A closer look at the coarse gimbal drives revealed several changes in requirements, from the ones originally considered, that make the stepper motor unsuitable. The detailed work* on the laser receiver using stepper motors and GTE image motion compensators (IMCs) has shown the importance of having a small step size to keep the tracking image within the dynamics of the IMC. This experience shows that the step size should be one-fourth the proposed 0.001°, which can be handled with greater gear reduction. However, two problems are to be considered: 1) wear life of the high speed end of the gear train, and 2) stepper motor torque is limited at high speeds now

*Contract NAS5-21854

required for slew modes. The reduced step size could be accommodated using the 1.8° PM stepper motor if a 90 day mission and slew rates 5 deg/min were acceptable. These parameters are probably acceptable for just the shuttle application. Since every parameter is near its physical limit, there is no room for growth in life, slew rate, or a more reduced step size. For this reason, the baseline design is changed to use a direct drive brush torque motor.

The direct drive motor selection allows slew rates to go up to the 140 deg-min shown as a possible requirement* in the First Quarterly Report with almost infinite resolution. The stepper motor system is generally chosen to minimize the electronic complexity, but only a modest increase in parts count is required to close a rate loop for the brush type torquer planned. Brush wear life is of little concern with only 16 rev/day and dry lubricated brushes will reliably operate for a few million revolutions. A brushless motor could be used but is not recommended because of the electronic complexity required to commutate the motor. The electrical power will probably be lower for this direct drive since the motor will be very much derated for the bearing torques encountered. This change does not eliminate the need for gearing to operate the off-axis encoder and resolver. These gears can now be instrumentation type since there is no high torque transmission, and also the antibacklash type gears may replace the negator preload spring.

5.2 IMAGE MOTION COMPENSATION

The presently used technique** for fine bearing control works well for a small field of view (~0.1°) acquiring a slow moving target. This technique, however, is not suitable for the case of a 1° FOV acquiring a fast moving target. To accommodate the larger FOV, it is necessary to go from piezoelectric devices to electromagnetic (EM) devices. The power consumption of the EM devices on the other hand should be kept within reasonable bounds requiring a scan frequency below 200 Hz. This is not compatible with the higher target rates using the present acquisition concept.

To reconcile the conflicting requirements, the acquisition concept in 3.2 is proposed. This new approach differs from the current approach in several ways. First, in order to reduce the apparent target motion, the gimbals are programmed to track out the known motion of the target. Second, in order to provide margin to the acquisition capability, a simple five-position gimbal scan is incorporated which is added to the programmed target motion. Third, in order to relax the IMC readout requirements, two IMC scan levels are used: a large scan covering the 1° field which requires no fine

*For the shuttle to ground link for a shuttle in a circular orbit at an altitude of 100 km.

**This technique is used in the optomechanical subsystem of a 10 μm receiver terminal developed under Contract NAS5-21859.

readout capability and a miniscan covering a 0.1° field which requires a readout accuracy of a few arcseconds. Last, the IMC position at the time the target is detected is stored as a reference for reacquisition on a second pass, rather than requiring the IMC to stop on target as is presently done.

5.2.1 IMC Requirements

The IMC requirements are defined by the IMC scan frequency, IMC scan amplitude, the size of the IMC mirror, and the resolution and accuracy of the IMC readout device. The scan frequency is somewhat independent of the other requirements and will be considered separately.

Scan Frequency

The scan frequency is determined by the target velocity and line resolution. The line resolution depends on the aperture size, which determines the angular subtense of the image. For the present 7 inch system, Hughes has a 3 dB beam diameter of approximately 0.004°, giving 125 diameters in 0.5° radial line.

The effective target velocity is composed of the actual target velocity minus the target velocity removed by the gimbal command sequence plus the body motion (unwanted) of the shuttle plus the spiral rate. For the backup acquisition mode in which the circular fence is used, only the shuttle rate and actual target motion are involved. The maximum target motion (at 60° zenith) is 0.24 deg/sec which, when added to the 0.01 deg/sec shuttle rate, gives a total rate of 0.25 deg/sec. Therefore, for this case the target will cross the detector in 0.016 second. If a 50 percent line margin is used, the line period is 0.008 second, which gives a required scan frequency for this case of 125 Hertz.

For the primary acquisition mode most of the target velocity is removed by the gimbal command sequence. The residual velocity, which depends on the command update frequency, is approximately 0.02 deg/sec for an update frequency selected to produce a residual error of 0.1°. Combining this with the 0.01 deg/sec shuttle rate gives a total velocity of 0.03 deg/sec plus that contributed by the spiral rate. The spiral rate is determined by the IMC scan period, which must be related also to the gimbal scan period. For the gimbal scan routine illustrated in Figure 3-5, the target should not be allowed to move more than approximately 0.6° during a gimbal scan period, which at 0.03 deg/sec requires a period equal to or less than 20 seconds. The IMC scan period should be no greater than one-fifth the gimbal scan period; that is, no greater than 4 seconds.

On the other hand, a scan frequency of 125 Hz, with a 50 percent line overlap, will cover the 0.5° in 2 seconds which produces an additional target velocity of 0.25 deg/sec. Therefore, it is proposed that the IMC scan period be increased to 4 seconds, thereby giving additional margin in case the shuttle and/or gimbal residual rates are larger than estimated.

In summary, the IMC scan frequency is chosen to be 125 Hz, with an IMC scan period of 4 seconds, and the gimbal scan period is equal to 20 seconds.

IMC Actuator

The size of the IMC mirror is determined by the ratio of the aperture to the magnification, whereas the mirror angle is determined by the product of the telescope FOV and magnification. Therefore,

$d_M S_M = D(FOV)$

d_M = IMC mirror diameter

A_M = IMC mirror angle

D = telescope aperture

FOV = telescope FOV

The required FOV is $\pm 0.5^\circ$ and the aperture diameter D is 7 inches. Thus, $d_M A_M$ is 3.5 inch-deg. For the PZT IMC presently used, $d_M A_M$ = 0.25 inch-deg, which product is low by a factor 14. Therefore, use of the PZT devices is out of the question for the transmitter, since an order of magnitude improvement in these devices is not possible.

Since the PZT device cannot be used, the next logical choice is an electromagnetic actuator driving the IMC mirror mounted on a flex pivot. These devices can be driven in the galvanometer mode or the servo mode. For the galvo mode the selected resonant frequency of the mirror/flex pivot combination is far enough above the driving frequency so that the mirror angle follows the torque input with little lag. In the servo mode the resonant frequency is chosen well below the drive frequency so that the flexures act as frictionless pivot bearings, and the mirror position is controlled through a servo loop. The latter operational mode is more complex but requires less power. The purpose of the following is to investigate the power and torque relationships in terms of the appropriate system design parameters.

The peak torque as a function of drive frequency ω is

$$T_{PK} = JA_M\omega^2\left[\left(\frac{\omega_n}{\omega}\right)^2 - 1 + \frac{j2\xi\omega_n}{\omega}\right] \text{ ft-lb} \qquad (5\text{-}1)$$

and the peak power is

$$P_{PK} = \frac{T_{PK}\omega A_M}{2} \text{ ft-lb/sec}$$

J = inertia

ξ = damping ratio

The power is plotted as a function of frequency in Figure 5-1. The numerical values used are based on the specific amplitude, damping ratio, and inertia given in the figure. A total power curve is given for a resonant frequency of 33 Hz and also for 500 Hz. These values are based on a required drive frequency of 125 Hz and represent, respectively, the case of servo operation and galvo operation. That is, for servo operation the resonant frequency is chosen a factor of 5 below the drive frequency, and for galvo operation the resonant frequency is chosen a factor of 4 above resonance. The third curve given is the power required simply to accelerate the inertia, which is proportional to frequency cubed. Both the other curves asymptotically approach the inertia curve for high frequencies. For servo case shown, for example, the total required power at the drive frequency is essentially the power required to accelerate the inertia on a set of frictionless bearings.

It is also obvious from Figure 5-1 that use of the galvo approach requires approximately a factor of 15 more drive power than does the servo approach. This fact is true, independent of the specific drive frequency and inertia used, as long as the proper resonant frequency-drive frequency separation is maintained. However, this fact in itself does not rule out use of the galvo approach. The numerical values used are based on a combined mirror-motor armature inertia of 10^{-4} lb-in-sec^2, most of which is due to the armature inertia and which is very sensitive to the particular magnetic design configuration. The selected value is also very conservative. Therefore, it might be possible to design a galvo type drive for which the power consumption would not be unrealistic.

General Parametric Relationships

The numerical values used in the above sections are generally based on specific values for the telescope aperture (7 inches), target velocity (0.25 deg/sec), telescope FOV ($\pm 0.5°$), telescope magnification (7x) and IMC mirror amplitude ($\pm 1.75°$). The above parameters are not all independent, but it is possible, by combining equations, to develop part of the parameters as if they are independent and to write the power and torque requirements in terms of these. For example, the three parameters D (telescope aperture), d_M (IMC mirror diameter), and V_T (target velocity) can be treated independently. D is chosen on the basis of the required optical link power, independent of the other two parameters. Similarly, V_T is "chosen" by selection of the acquisition approach as discussed in 3.2. Also d_M can be varied by changing the telescope magnification. Obviously there are constraints on these parameters. If d_M is too small (much below an inch, for example) the

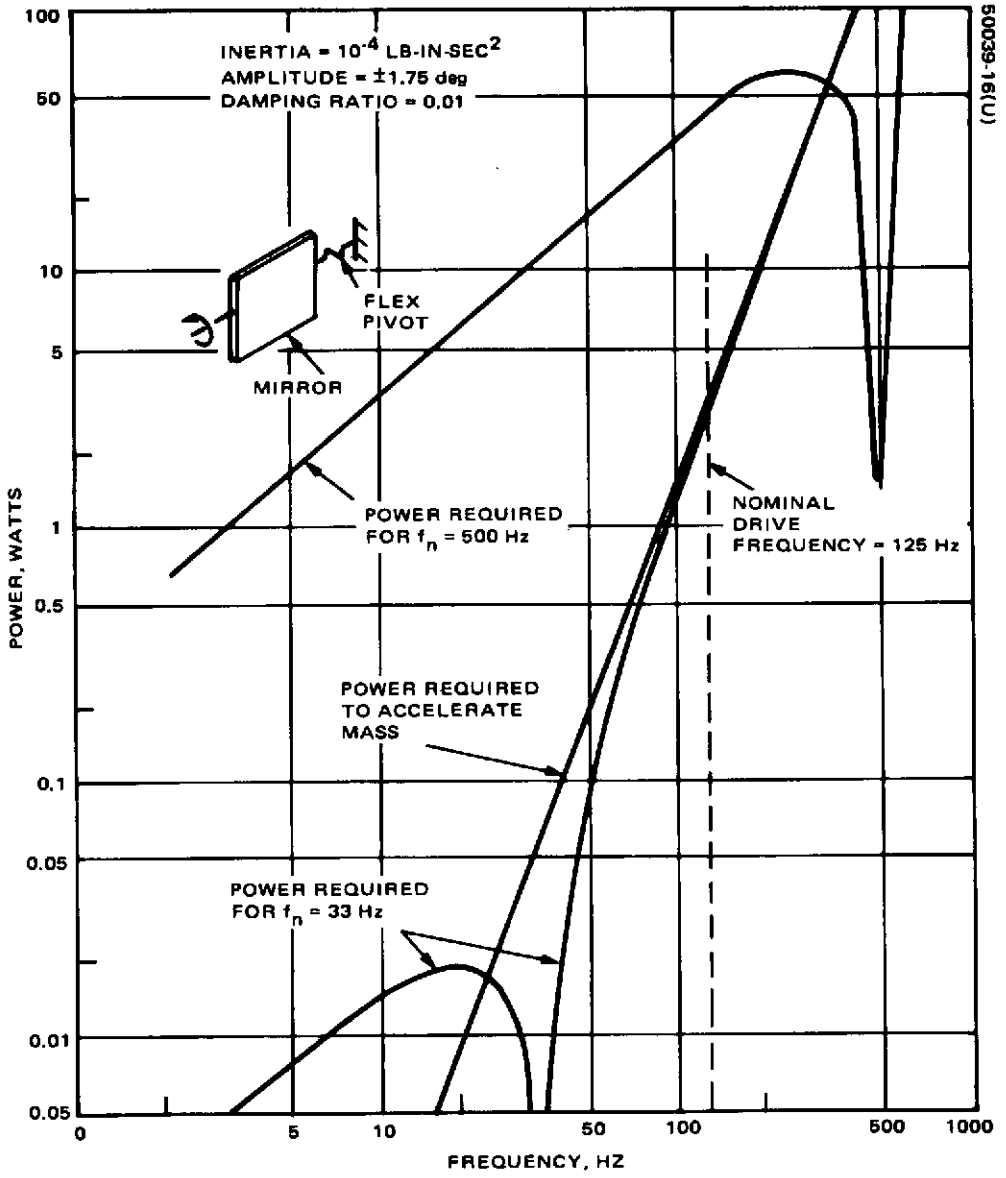

FIGURE 5-1. MECHANICAL POWER VERSUS DRIVE FREQUENCY FOR FLEX PIVOT MOUNTED MIRROR

optical design will be unduly complicated. However, these parameters can be varied over particular ranges and it is instructive, therefore, in optimizing the overall system to determine how the power, torque, and drive frequency depend on these three parameters.

First, the inertia of IMC mirror and rotor is written in terms of the mirror diameter.

$$J = K_1 d_M^5 \tag{5-2}$$

The above equation assumes that 1) the mirror thickness is related directly to its diameter and 2) the total IMC drive inertia is directly proportional to the mirror inertia. Also, the mirror amplitude is related to the FOV, d_M, and aperture D as discussed above,

$$A_M = D(FOV)/2d_M \tag{5-3}$$

The maximum velocity is expressed as

$$\dot{\theta}_{MAX} = \omega A_M$$

which gives the required drive frequency ω in terms of V_T and D as

$$\omega = K_2 V_T D \tag{5-4}$$

D is in feet, V_T in deg/sec and ω in rad/sec. For the resolution requirements discussed above,

$$K_2 = 5582, \text{ and} \tag{5-5}$$

$$\dot{\theta}_{MAX} = (24.35)\ \frac{D^2 V_T}{d_M}$$

and the peak torque is

$$T_{PK} = K_3\, d_M^4\, D^3 V_T^2 \text{ ft-lb} \tag{5-6}$$

For the servo case, assuming $\omega_n = \omega/5$,

$$K_3 = 2.82 \times 10^5 \tag{5-7}$$

The peak power is expressed as

$$P_{PK} = K_4 D^5 V_T^3 d_M^3 \text{ watts} \tag{5-8}$$

where $K_4 = 4.67 \times 10^6$ for the above set of assumptions plus the added assumption that the peak power is half the product of peak torque and peak velocity, since the latter two are approximately 90° out of phase.

The above equations show that the power required to drive the IMC mirror is very sharply dependent on the aperture size. Increasing the aperture from 7 to 9 inches will increase the power requirements by a factor of 3.5. This is because both the scan frequency and scan amplitude decrease with decreasing aperture.

5.2.2 Servo System Block Diagram

A block diagram of the servo system is given in Figure 5-2. As discussed previously, the position of the target relative to the detector is difference between the gimbal motion and the target motion summed with the IMC position. Initially, the IMC position is scanned in a spiral scan over the entire telescope field of view (± 0.5°). After the first acquisition pulse, the IMC scan field of view is reduced by a factor of 10 to ± 0.05° (miniscan), in response to acquisition discrete A3. At the same time two other things happen. First, the gimbal scan is turned off and second, an increment is added to the gimbal position in order to bring the target closer to the center of the IMC FOV. The required increment is obtained by sampling the IMC position at the instant of threshold detection. A third item, not illustrated in the diagram, may be required: change of the scale factor in the IMC loop to reduce its dynamic range by a factor of 10, thereby improving its resolution.

When the target is acquired in the miniscan mode, a second discrete A2 is generated. This causes the IMC position to be sampled at the instant the acquisition discrete is obtained, and the IMC loop subsequently to be commanded to the measured IMC position. The track scan (conical scan) is also enabled by the A2 discrete. Thus, acquisition of the target in the miniscan mode (fine acquisition) causes the IMC loop to "back" the target to the detector at which point a track error signal should be developed. The track error produces the fine track discrete A3 which closes the fine track loop. A few milliseconds later, after the fine track loop has settled, the delayed fine track signal is produced, which closes the gimbal IMC loop. This completes the acquisition procedure.

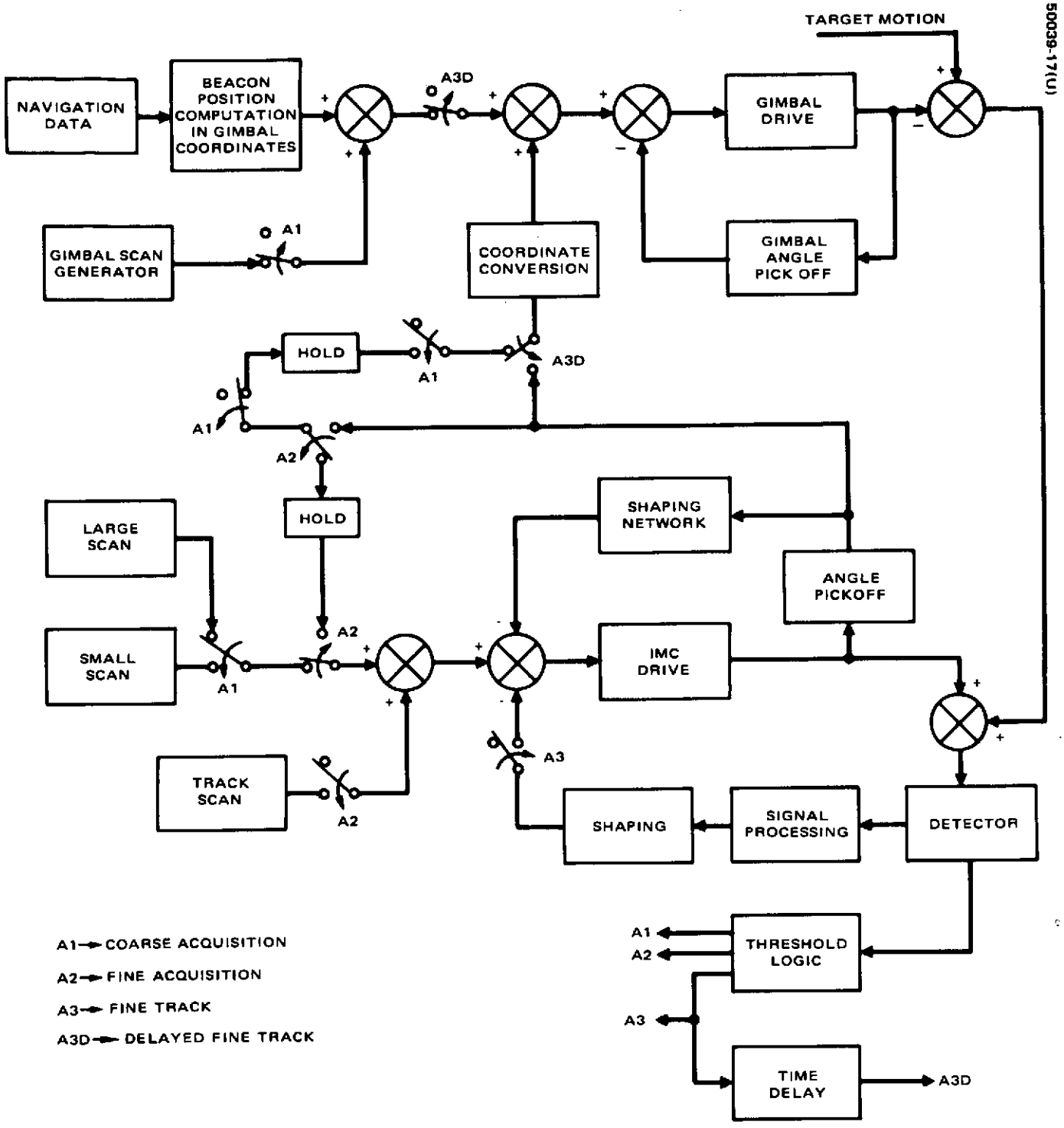

FIGURE 5-2. SIMPLIFIED ACQUISITION/TRACK DIAGRAM FOR SHUTTLE TO GROUND LINK

6. EXPERIMENT MEASUREMENT OF OPTOMECHANICAL SUBSYSTEM OF 10 μm RECEIVER

The purpose of this task is to integrate the waveguide local oscillator, the servo drive electronics, and the AIL receiver and doppler tracking electronics into the optomechanical subsystem (OMSS) to provide a complete optical heterodyne receiver, and to test and evaluate the completed receiver to determine its performance characteristics. The listed components to be integrated were developed under contracts NAS 5-21859, NAS 5-23119, NAS 5-23183, and NAS 5-23211.

Work was initiated the month of October 1974. During this month, special test and support fixtures were designed and ordered, the AIL receiver electronics were received, a 10.6 micron large aperture collimator was assembled, and, at the contract monitor's request, a spare HgCdTe detector was ordered and received from SAT. In addition, the optical alignment and testing of the OMSS and the electrical testing of the servo system have been monitored to assess the status and performance of these subsystems.

A special cart for mounting the OMSS has been ordered. The OMSS will be mounted to the cart top under a lucite dust cover. The cryostat control and monitoring panels, the receiver front end control panel, and the local oscillator power supply and frequency control electronics will be mounted on the side of the cart. A bracket at one end of the cart will be fabricated to hold the required high pressure nitrogen supply. Mechanical jack screws will be located at the four corners to lift the cart off the casters for increased rigidity during optical testing.

The AIL equipment was received from Goddard along with the Tau-Tron bit error rate (BER) test set near the end of October. The equipment has been unpacked and visually inspected and initial operation of the Tau-Tron equipment has been completed. Mounting racks for the equipment have been ordered.

It has been determined that sufficient funding still exists in the local oscillator contract to furnish a regulated power supply for the tube, and to fabricate a Stark cell and the associated electronics to provide a fully stabilized laser with provisions for setting the frequency anywhere within the oscillating range on the P20 or P14 transitions. These additions will facilitate measurements during acquisition tests on the completed receiver.

The OMSS has been assembled and aligned, and basic optical testing has been completed. The electronics for the servo system are undergoing modifications to prevent inadvertent damage to optical components.

During the month of November, some of the special test fixtures were received, the servo system was operated against a visible laser source, the AIL receiver was characterized, and the waveguide local oscillator was received.

The aluminum cart for the OMSS was received near the end of this month, and modifications have begun. Four jackscrews have been installed to lift the cart off its casters during the testing. A lucite cover has been fabricated for the OMSS. Brackets for mounting the high pressure nitrogen bottle to the cart have been received and will be mounted during the next period. The cart will be modified to accept standard rack panels, and the cryostat control panel, detector temperature monitoring panel, receiver front end control panel, laser control oscillator power supply, and laser frequency control panel will be installed. The remainder of the electronics will be installed in the control console.

A silicon detector and field stop have temporarily been installed on the OMSS. This has allowed operation of the pointing and tracking system in conjunction with a HeNe laser and 20 inch collimator. The OMSS is installed on a precision rotary table (Fecker table) to provice calibrated angular motion. Qualitative testing of the acquisition and tracking functions indicates that the system will exceed its functional requirements by a comfortable margin. Quantitative measurements have been hindered by lack of a calibrated rate drive for the Fecker table, but alternative means of making these measurements are under investigation.

The AIL receiver has been exercised and appears to meet or exceed its specifications. (The cryostat has not been operated, nor has the SAT detector.) One problem has been discovered in the AGC system. The AGC appears to have a nonlinear fast attack/slow decay characteristic caused by some protective circuitry built into the AGC control amplifiers. While this does not affect operation of the demodulation function or the doppler tracking function, it does cause a nonlinear response to amplitude modulation. Since the conical scan tracking system relies on this information, acquisition and tracking error distortion in the 150 Hz conical scan signal will cause a tracking error in the servo loop. AIL has been contacted regarding this problem, and modification of the ATC circuitry has been initiated. A second set of AGC amplifiers will be fabricated by Hughes to alleviate the problem, thus maintaining the present AIL AGC amplifiers intact for comparison purposes.

The waveguide local oscillator has been received and fitted into the OMSS package to check interfacing. No problems were encountered. The Stark Cell for the laser has been fabricated and tested, and the electronics for frequency control are under construction. The laser has been returned to the Research Labs for integration with the Stark Cell and electronics.

The first 2 weeks of December were devoted to "show and tell," with the spatial acquisition and tracking subsystem, the doppler tracking and data demodulation subsystem, and the local oscillator and Stark Cell placed on display for upper management and outside visitors. The system was well received, and in keeping with the schedule, no significant delays have been encountered.

During the lulls between visitations, the quantitative tests on the servo subsystem were completed.

The remainder of December (less the end-of-year holidays) was devoted to preparing the system for 10.6 micrometer testing, scheduled for April. The following tasks were accomplished:

- Most of the components have been mounted on the test cart, including the high pressure N_2 supply and the cryostat control panels. A plexiglas dust cover for the OMSS has also been fabricated.

- A new set of AGC amplifiers for the doppler tracking electronics has been breadboarded. These amplifiers eliminate the distortion evident on the 150 Hz conical scan signal and improve signal leveling by incorporating integrators into the loops.

- A mounting system for the cryostat and for an alignment pinhole has been devised that will allow interchanging the two elements without loss of alignment. Most of the parts for this mechanism have been fabricated.

- A preliminary optical layout for the local oscillator conditioning optics has been completed.

- The Stark Cell electronics for the local oscillator have been breadboarded and tested.

7. REFERENCES

1. B.J. Klein and J.J. Degan, "Optical Antenna Gain. 1: Transmitter Antennas," Applied Optics, September 1974.

2. B.J. Klein and J.J. Degan, "Optical Antenna Gain. 2: Receiving Antennas," Applied Optics, October 1974.

3. D. Dalian, "Degradation in Digital Communication Systems Due to Bandwidth Restriction," Hughes Aircraft Company, Interdepartmental Correspondence, 8 July 1974.

4. "Experiment Definition Phase, Shuttle Laboratory, LDRL 10.6 Experiment," First Quarterly Report, Hughes Aircraft Company, 15 October 1974.

5. "NASA Laser Data Relay Link (LDRL) Experiment for the DOD/NASA Cooperative Space Laser Communication Test Flight," Volume III, Appendix A, Goddard Space Flight Center, Greenbelt, Maryland, May 1974.

6. "Space Shuttle System Payload Accommodations. Level II Program Definition and Requirements," Volume XIV, Revision C, pages 3-9.

7. W.N. Peters and A.M. Ledger, "Techniques for Matching Laser TEM_{oo} Mode to Obscured Circular Aperture," Applied Optics, 9 June 1970, pp. 1435-1442.